5-2007

Thin Film Solar Cells Using ZnO Nanowires, Organic Semiconductors and Quantum Dots

Kaitlyn VanSant
Portland State University

THESIS APPROVAL

The abstract and thesis of Kaitlyn VanSant for the Master of Science in Physics were presented May 11, 2007, and accepted by the thesis committee and the department.

COMMITTEE APPROVALS:

[redacted]

Rolf Könenkamp, Chair

[redacted]

Rajendra Solanki

[redacted]

Andres LaRosa

[redacted]

Carl Wamser
Representative of the Office of Graduate Studies

DEPARTMENT APPROVAL:

[redacted]

Erik Bodegom, Chair
Department of Physics

ABSTRACT

An abstract of the thesis of Kaitlyn VanSant for the Master of Science in Physics presented May 11, 2007.

Title: Thin Film Solar Cells Using ZnO Nanowires, Organic Semiconductors and Quantum Dots.

A thin film organic/ inorganic hybrid solar cell was fabricated by incorporating ZnO nanowires, n- and p-type organic semiconductors and inorganic quantum dots. The basic cell design involved the electrodeposition of ZnO nanowires grown on a substrate coated with a transparent conductive oxide. The ZnO nanowires were coated with a thin layer of an organic n-type material, followed by a deposition of inorganic quantum dots. A p-type polymer layer was subsequently deposited and the sample was then contacted with gold to form a quantum dot layer sandwiched between a p-n junction of organic conductive materials.

Various materials and processing methods were adjusted, using I-V characteristics, photovoltage and/ or photocurrent measurements to determine the performance of the cell. Each constituent material in the basic device design was evaluated in terms of its contribution to the sample characteristics. A variety of deposition techniques were investigated to obtain homogeneous layers. Different

annealing procedures were explored with the intent of balancing the time and temperatures required for electrical activation with material constraints such as tendency towards oxidation and low melting points. The effect of time on the sample characteristics was also observed. The evaluation primarily includes data for samples that led to design modifications aimed at improving both electrical properties and quantum efficiencies.

This research led to the development of a hybrid solar cell sensitized by the addition of quantum dots. The organic semiconductors were used to form a p-n junction, and the p-type polymer also served as an active absorber layer. The quantum dots were used as the inorganic absorber layer, and the results show that the range of optical absorption in the cell can be modified by adjusting particle size. In addition, the ZnO nanowires appear to improve charge transfer, when used with materials that have favorable band offsets.

THIN FILM SOLAR CELLS USING ZNO NANOWIRES, ORGANIC SEMICONDUCTORS AND QUANTUM DOTS

by

KAITLYN VANSANT

A thesis submitted in partial fulfillment of the
requirements for the degree of

MASTER OF SCIENCE
in
PHYSICS

Portland State University
2007

ACKNOWLEDGEMENTS

My most sincere appreciation goes out to the following individuals:

- **Dr. Rolf Könenkamp for coming up with the concept for this project, allowing me to work on it, and for all of the knowledge and advice he has passed along in the process. With respect to this thesis, I greatly appreciate his editing, clarification of ideas, and especially his patience.**

- **Dr. Robert Word, for in-lab training, device improvement recommendations and for his knowledge and advice in the field of physical chemistry. I am also grateful for his edits and recommendations for this paper, and his graphic design expertise.**

- **Athavan Nadarajah for in-lab training, multiple ZnO samples, and for his suggestions on this project.**

- **Dr. Carl Wamser, for allowing me to attend his research group meetings, loaning me reference materials, and participating as a member of the thesis committee.**

- **Dr. Andres LaRosa and Dr. Rajendra Solanki for participating on the thesis committee.**

TABLE OF CONTENTS

LIST OF TABLES

LIST OF FIGURES

1. Introduction

1.1 Motivation for research

There is currently a strong trend towards diversifying away from traditional energy resources and instead focusing on renewable alternatives to fossil fuel and nuclear sources. Solar power is particularly appealing, but the challenge is to find the technology that can utilize this readily available energy that is already globally distributed.

The main goal of solar cell design is to maximize efficiency. For large scale manufacturing feasibility, however, the quest for higher efficiency is tempered by considerations of material and production costs. Unfortunately, the current tendency is for costs to increase with efficiency, and vice versa. Finding the optimum balance between efficiency and cost is the primary goal of today's solar power industry.

In the research presented herein, all materials are deposited at room temperature on low-cost substrates. The organic materials are also low-cost, and the inorganic nanocrystals have the potential to be inexpensive, if produced in-house. Another advantage is the relative ease of processing, compared to the high vacuum/ high temperature fabrication procedures necessary for standard crystalline silicon cells.

The principal goal of this research, however, is the pursuit of higher efficiency. This thesis addresses thin film organic/ inorganic hybrid solar cells. The prepared samples primarily incorporate ZnO nanowires, n- and p-type organic semiconductors and inorganic quantum dots.

1.2 Overview of Photovoltaic Theory

A photovoltaic cell converts light energy into electrical energy. A solar cell is a photovoltaic device that is specifically designed so that maximum light absorption occurs in the solar spectrum (See Figure 1).

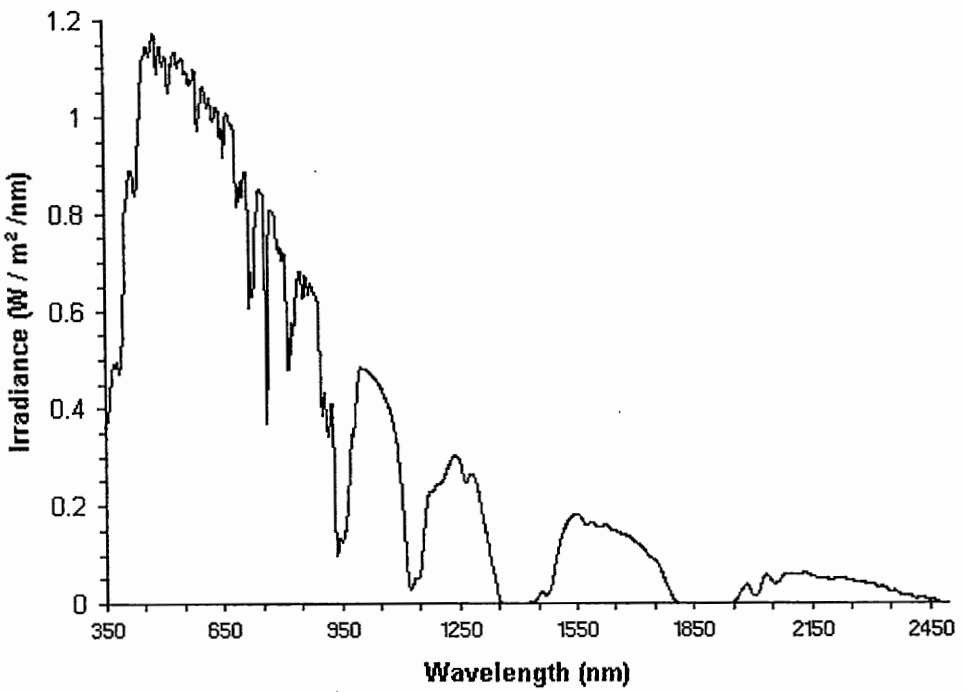

Figure 1.1 Solar spectrum

The majority of commercially available solar panels are silicon based. Second and third generation photovoltaic technologies rely on a variety of semiconductor materials, such as conductive polymers, nanoparticles and organic dyes. Materials that absorb at different wavelengths can be layered in a single device to create a broader spectral response.

The primary functions of a photovoltaic device are (1) photogeneration of electron-hole pairs in a light absorbing material, and (2) the separation and conduction

of those charge carriers to contacts that transmit the current out of the cell. A photon may be absorbed by a photovoltaic semiconductor if it has enough energy to create an electron-hole pair in the material. The minimum energy for absorption depends on the bandgap (E_g) of the material, which is the energy required to excite an electron to the conduction band (E_c) and leave a hole in the valence band (E_v): $E_g = E_c - E_v$.

The Fermi level (E_f) represents the transition between occupied and empty states. The occupation probability at E_f is 50%. In semiconductors, E_f is in the bandgap, so there are few electrons free to move into the conduction band states. The Fermi level can be modified by doping, which involves the intentional introduction of impurity atoms.

Once the electron-hole pair has been generated, the carriers must be separated and transmitted to their respective electrical contacts. Charge separation is often enhanced at the interface between two materials because of the presence of built-in electric fields (V_{bi})

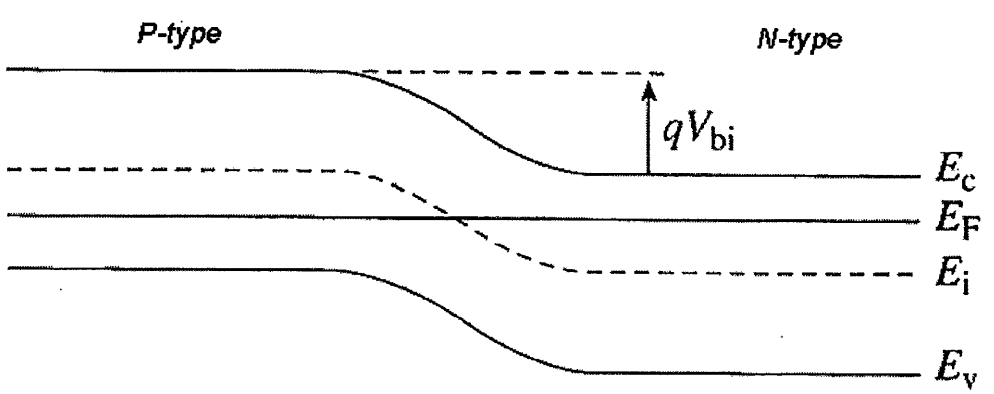

Figure 1.2 Equilibrium energy band diagram.

1.3 Efficiency

The quantum efficiency of a solar cell is the ratio of output electrons to incident photons. The quantum efficiency is useful in characterizing and analyzing the operation of the device. The energy conversion efficiency quantifies the useful performance of the solar cell as a power source. It is always lower than the quantum efficiency, since the electrons lose a substantial portion of their energy in a variety of avoidable and unavoidable processes. Thus while the number of collected electrons may well be equal to the number of incident photons (making the quantum efficiency equal to one), there is always a substantial reduction in electron energy (making the energy conversion efficiency smaller than one).

There are numerous factors that can reduce the efficiency of a device. On one hand, the film must be thick enough to absorb most of the incident light. On the other hand, there is a finite probability of recombination of the excited electrons and holes subsequent to the excitation process and during the transport process through the device. Losses may also occur due to inefficient charge transfer at various layer interfaces, and the presence of impurities. These effects may technically be avoided by improving contact formation, reducing impurity and defect densities and increasing charge carrier mobilities.

Other loss mechanisms appear more fundamental. Thermalization and absorption losses occur even in ideal devices as incident photons must have enough energy to be absorbed, and excited electrons will dissipate some of their excess energy by bringing themselves into thermal equilibrium with the crystal lattice by transferring

energy into lattice vibrations and by electron scattering processes. These processes are known as thermalization, and constitute a large factor contributing to low energy conversion efficiencies. These processes are unavoidable in the conventional single-junction solar cell design. They are a consequence of using a two-level system consisting of conduction and valence bands to harvest a broad distribution of photon energies. In addition to thermalization, there is also an unavoidable loss due to increased radiation from the solar cell [1]. Shockley and Queisser predicted in 1960 that, based upon the unavoidable physical limitations addressed above, the maximum efficiency of a silicon-based p-n junction solar cell would be 31% [2].

Shockley and Queisser's predicted efficiency limits, however, pertain to devices composed of a single semiconductor material in the active region. In first generation photovoltaics, this single material was high quality crystalline silicon, but material and processing costs for this technology are expensive. The second generation focuses on semiconductor thin films that can be fabricated using less material and less stringent processing methods, thereby significantly reducing both the mass of the device and the manufacturing costs. Multiple-junction thin film solar cells with high efficiencies were initially envisioned, but efficiency has remained low due to a higher defect concentration associated with the lower processing standards. Third generation devices aim to incorporate novel materials that do not depend on conventional p-n junctions to separate carriers, such as conductive polymers, nanoparticles and light-absorbing dyes. Other third generation projects aim at pushing the theoretical efficiency limits confronting single material devices by increasing

absorption, reducing thermalization and addressing sub-band gap losses (i.e. tandem cells, hot carrier cells, etc.) [3]. Research presented in this thesis involves both second and third generation concepts.

1.4 Envisioned Device

The research for this thesis aims at developing a photovoltaic device that incorporates organic semiconductors, ZnO nanowires and inorganic quantum dots. The ZnO nanowires are grown on a FTO (Fluorine-doped SnO_2) substrate by electrodeposition. FTO is the cathode of the device. The nanowires are spin-coated with a thin layer of n-type material, then an absorber layer of Cadmium-based nanoparticles is drop-coated. The sample is then spin-coated with a p-type polymer, followed by a gold top contact that forms the anode.

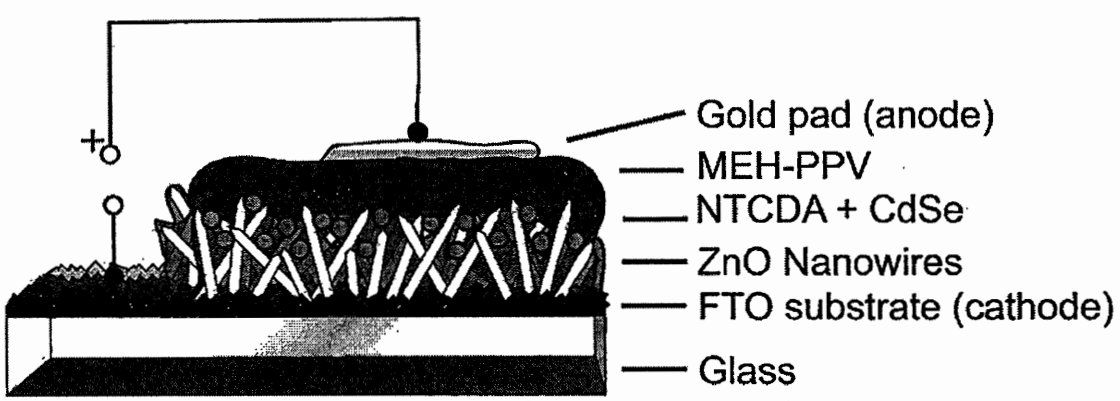

Figure 1.3 Basic design of photovoltaic device.

When light is incident upon the device, the main absorption occurs both in the quantum dot layer and the p-type polymer. The p-type polymer transports the holes to the anode, while the electrons are conducted through the n-type material to the ZnO nanowires, which then transports them to the FTO cathode.

1.3.1 Background on ZnO nanowires

The foundation for this solar cell design is based upon previous research done on light emitting diodes (LED) fabricated by the electrodeposition of ZnO nanowires on FTO, insulated by polystyrene, then coated by the hole-injecting polymer poly(3,4-ethylenedioxythiophene) (PEDOT-PSS), and contacted with gold [4]. The general design of this LED is transferable to a photovoltaic cell. The purpose of using the ZnO nanowires in the solar cell design is to establish a high mobility pathway for electron transport from the absorber region to the FTO contact layer. In our most recent photovoltaic samples, the ZnO nanowires were grown with low concentrations of $AlCl_3$ in the electrodeposition solution in order to make the ZnO slightly n-type and more conductive [11].

1.3.2 Organic semiconductors

Many organic semiconductors (also referred to as conductive polymers) can be dissolved and processed as a liquid at room temperature, which allows for inexpensive spin coating depositions and the possibility of large scale depositions by ink-jet or screen printing. Layers of conductive polymers could be used to accommodate photon absorption at different wavelengths in order to increase efficiency, analogous to hetero-junction inorganic solar cells. The main difficulties with organic semiconductors are their low electron and hole mobilities and the tendency to degrade quickly with exposure to light, oxygen and humidity (this will be addressed in more detail later) [5].

Organic semiconductors conduct on account of their conjugated structure. The framework consists of alternating single- and double- carbon-carbon bonds that lie along the polymer backbone. Conjugated polymers have a single bond backbone along which the carbon sp^2 hybrid orbitals overlap. This results in the formation of π-bonds between the overlapping p_z orbitals that remain out of the plane of the polymer. The electrons in these p_z orbitals, however, are delocalized over the entire molecule. The overlapping p_z orbitals produce a lower energy π-orbital (also known as the highest occupied molecular orbital or HOMO level) that acts as the valence band, and a higher energy π^* orbital (known as the lowest unoccupied molecular orbital or LUMO level) that behaves as the conduction band, thus forming a band gap similar to that of an inorganic semiconductor. Most conductive polymers have band gaps between 1.5-3 eV, which is an optimal range for absorption of sunlight [6].

When a photon is absorbed in a conductive polymer, an electron is excited from the valence band to the conductions band, but then diffuses through the polymer as an exciton, or a coupled electron-hole pair. When the exciton reaches an interface, it can be split into a separate electron and hole, and the separated carriers can then be driven out of the cell by the internal electric field at the interface between materials with different work functions.

This conduction mechanism accounts for a significant portion of conductive polymer inefficiencies. Polymer excitons have short lifetimes and easily recombine before reaching an interface. This is often worsened by the presence of impurities such as oxygen, which can act as a trap for the diffusing excitons. In addition, the

exciton-splitting process at material interfaces is not very efficient. Investigations into methods for mitigating these problems are ongoing, but the energy conversion efficiencies of polymer-based photovoltaic devices have remained substantially less than that of their inorganic counterparts [7].

1.4.3 Quantum Dots

We used commercial quantum dots as the inorganic absorber material in our standard cell design. Both CdSe and CdTe were investigated, with CdSe-based cells exhibiting the best results.

Quantum dots exist between the molecular and sold-state regimes, and thus their electronic and optical properties are largely determined by their size and shape. On the macro-scale, electronic behavior is well described by band structure models for semiconductors but, as the particle size approaches that of a molecule, deviations from these models become quite pronounced and changes in the density of states distribution energies become apparent. In particular, there is an increase of the band gap with decreasing particle size, requiring more energy for electronic excitation.

In a quantum dot, the carriers are confined to a small volume, which can be described as an infinite potential well of width d, corresponding to the diameter of the particle. For a semiconductor quantum dot, the minimum energy E_g necessary for creating an electron-hole pair must take into account numerous factors. For a basic approximation of the band gap:

$$E_g(\text{quantum dot}) = E_g(\text{bulk}) + E_{well} + E_{Coul}$$

E_g (bulk) represents the band gap of the bulk semiconductor. E_{well} is the energy associated with the confinement of the carriers to the potential well and varies as $1/d^2$. The Coulomb interaction E_{Coul} takes into account the mutual attraction between the electron and the hole, along with the screening effect of the surrounding crystal, and varies as 1/ d. The confinement energy is always positive, thereby increasing the band gap of the nanoparticle relative to E_g (bulk), but the Coulomb interaction is always attractive for the electron-hole pair, which lowers its energy. The quantum confinement effect influences the band gap considerably as the quantum dot diameter d gets smaller. In Figure 1.3, as the particle size decreases, the energy band gap increases along with the optical density. The fundamental absorption edge of the material is thus "blue-shifted" with decreasing particle size [8].

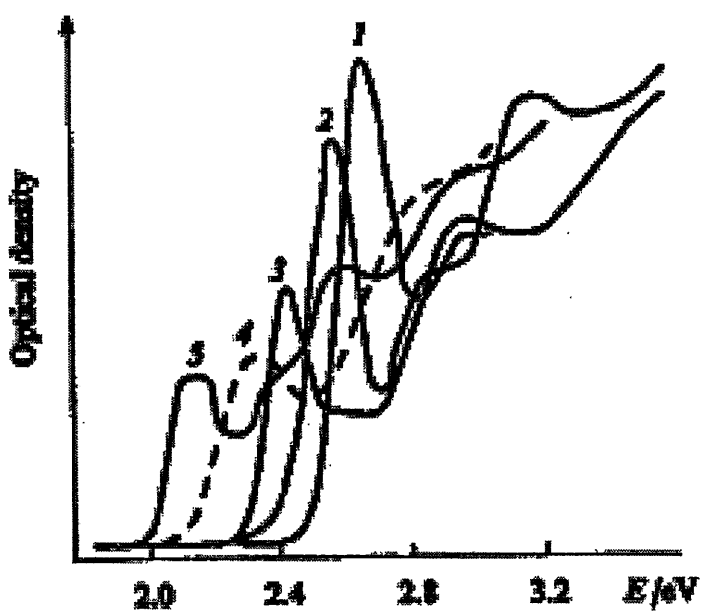

Figure 1.4 Absorption spectra of CdSe quantum dots of various sizes (nm): (1) 2.1, (2) 2.3, (3) 2.7, (4) 3, (5) 4

Quantum dot properties are also influenced by the ligands that isolate the individual particles. Without ligands, nanoparticles tend to have a high density of dangling bonds, which act as traps for charge carriers and increase non-radiative recombination rates. In addition, these dangling bonds are very reactive and lead to oxidation upon exposure to the atmosphere. This oxidation may further degrade the electronic and optical properties of the material. If the quantum dots are synthesized with protecting ligands, however, the dangling bonds can be passified and narrow particle size distributions can be obtained. Certain ligands can also make the particles more soluble in a variety of solvents. With a narrow size distribution of particles, the electronic and optical properties are well defined, and thus often more useful for device fabrication [9].

1.5 Objectives of Work

The goal of this research was to build a promising nano-structured solar cell. Each fabricated sample was then characterized, and compared to the characteristics of previous devices, with an eye towards refining the design for better efficiency.

Materials were chosen based upon their absorption profiles and n-or p-type properties, carrier mobilities, required annealing temperatures and the theoretical interfaces that could be obtained between layers. To obtain homogeneous layers, various solvents and deposition techniques were investigated, particularly for the inorganic materials. Although both the organic semiconductors and the quantum dots have promising photovoltaic properties, the goal was to improve absorption in the inorganic materials, to avoid degradation challenges confronting the organic materials.

Another significant parameter is layer thickness. Considerable effort went into optimizing layer thickness. Layers should be just thick enough to prevent electrical shorts, but also thin enough to maximize the number of photogenerated carriers. These investigations involved varying solution concentrations, solvent types and deposition methods.

Likewise, annealing procedures for composites of various materials must be carefully considered. Polymers typically have low melting points, which limits their feasibility as a material for front-end processing. Organic semiconductors must also be annealed in vacuum, since the elevated temperature will amplify the standard problem of oxidation. Cadmium-based materials, however, require high temperature anneals, preferably in air, if $CdCl_2$ is to be used for doping during annealing, as is often reported in the literature. It is critical to optimize this balance between the time and temperatures necessary for activation with concerns of material constraints.

In addition to efficiency improvements, the performance of each device was evaluated for insights into how the cell operates. Modifications that are not advantageous for optimizing characteristics may be useful in clarifying the function of a particular layer, or how it interacts with the other materials.

2. Experimental Methods and Materials

2.1 ZnO Nanowires

ZnO is a II-IV semiconductor with a bandgap of $E_g = 3.36$ eV (at 300 K), and an absorption peak at $\lambda = 368$ nm in vacuum [28]. It has a Wurtzite structure, as shown in Figure 2.1, which leads to the preferential growth of structures with hexagonal cross-sectional symmetry.

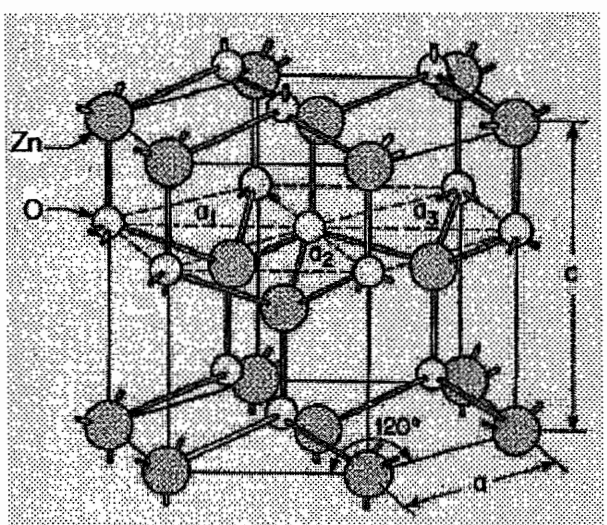

Figure 2.1 ZnO Wurtzite structure, with lattice constants a = 3.250 Å and c = 3.206 Å [28].

ZnO nanowires are electrodeposited on a Fluorine-doped SnO_2 (FTO) coated glass substrate (manufactured by Pilkington under the name "Tec 8"). We followed methods similar to those of Peulon and Lincot using a standard three-electrode electrodeposition process [10]. The FTO substrate is attached to a Pt wire to form the working electrode, the counter-electrode is a Pt foil and the reference electrode uses an Ag/ AgCl electrode (E_0 = 0.2V vs NHE) to maintain a constant potential. The electrodes are immersed in an aqueous solution that contains 3×10^{-4} M $ZnCl_2$ and 0.1 M KCl. During the deposition, oxygen is bubbled continuously into the solution, the

temperature is maintained at 80° C, and a –1.0 V vs MSE potential is applied for one hour by an EG&G Instruments Model 283 Potentiostat. Typical pH values ranged from 4.5 to 5.3.

Several competing reactions occur during the deposition that assist in transporting the Zn^{2+} ions to the solution/ substrate interface to obtain the following overall reaction:

$$Zn^{2+} + 0.5O_2 + 2e^- \rightarrow ZnO \{E_0 = 0.93V/NHE\}$$

This reaction is sensitive to minor changes in solution pH, $ZnCl_2$ concentrations, O_2 concentrations, temperature and potential.

One variation that was incorporated after Sample 78 was the addition of 5 μM $AlCl_3$ to the solution, which slightly increased the solution pH to 5.7. Incorporation of Al in ZnO growth has been shown to improve the electron mobilities in ZnO, suggesting that the nanowires become more strongly n-type [11]. Al-doping the ZnO may further assist the NTCDA in charge separation and improve electron transport to the FTO contact.

2.2 Organic Semiconductors Coatings

The conductive compounds were dissolved in solvents and deposited to form a p-n junction, with the nanoparticles sandwiched between the n- and p-type layers. Ideally the nanoparticles would absorb the incident light and generate the majority of the electron-hole pairs, transporting the carriers through the organic semiconductor layers to their respective contacts. Empirically, however, it was found that the MEH-PPV also exhibits a significant photovoltaic response.

Each organic layer was deposited by spin coating at 3000 rpm for 60 seconds. The concentration of each material in solution was varied and optimized to obtain both a homogeneous deposition and the thinnest possible layer that would be thick enough to prevent electrical shorts.

2.2.1 NTCDA

1, 4, 5, 8-Naphthalenetetracarboxylic dianhydride (NTCDA) is an n-channel organic semiconductor. The NTCDA was used to form a thin n-type wetting layer over the ZnO nanowires. It was incorporated to improve the contact between the subsequent layer of CdSe quantum dots and the nanowires, thereby assisting in electron transport. Due to its n-type conductivity, the NTCDA also forms a p-n junction with the MEH-PPV coating that is deposited on top of the CdSe.

This material was purchased from Sigma Aldrich and has a molecular weight of 268.18 amu.

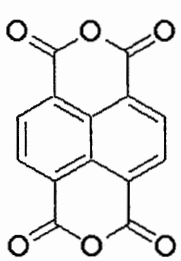

2.2 Chemical Structure NTCDA
Molecular Formula: $C_{14}H_4O_6$

There is some disagreement in the literature available on NTCDA over the bandgap values. A band gap of 3.3 eV was deduced based upon the absorption spectra by A. Nollau and G. Liang, but this value was deduced from highest occupied molecular orbital (HOMO) levels ranging from 6.9 to 8 eV and lowest unoccupied molecular

orbital (LUMO) levels of 3.6 to 4.7 eV (12, 13). The optical band gap itself ranged from 3.1 to 3.95 eV in the literature, and generally appears to be a difficult measurement to obtain with accuracy [12-15]. Electron mobility values for NTCDA were measured as 3 x 10^{-3} cm^2/ Vs in a field-effect transistor fabricated from NTCDA deposited at a substrate temperature of 55° C for a 12 μm channel length device and operated under vacuum, but the mobilities dropped by one to two orders of magnitude upon exposure to air [16, 17].

NTCDA was dissolved in DMSO at concentrations varying from 3 g/ L to 10 g/ L. The lower concentration was used to obtain a thin layer, so that the majority of generated carriers would be within the diffusion length of the interface between the NTCDA and the ZnO nanowires. The higher concentration, however, was investigated to determine if the thicker layer of NTCDA would form a better p-n junction with the MEH-PPV and therefore result in better rectification in the I-V curves. Post deposition, each sample was annealed in vacuum (1 torr) at an initial temperature of 300°C, and allowed to gradually drop back down to room temperature in vacuum.

2.2.2 MEH-PPV

Poly[2-methoxy-5-(2-ethylhexyloxy)-1,4-phenylenevinylene] (MEH-PPV) is a p-type light-emitting conjugated polymer often used in LED applications. It was purchased from Sigma-Aldrich, with an average molecular weight of 150,000-250,000 amu and a peak absorption of λ_{max} = 498 nm.

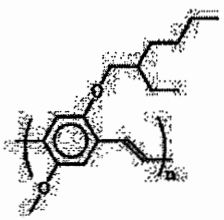

Figure 2.3 Chemical Structure of MEH-PPV
Molecular Formula: $(C_{18}H_{28}O_2)_n$

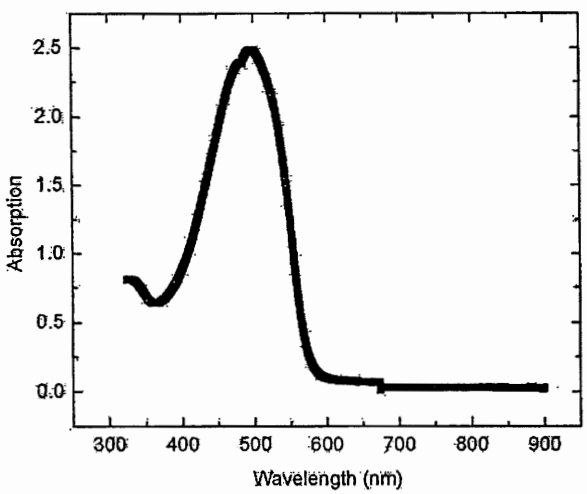

Figure 2.4 Typical Absorption Peak for MEH-PPV

Hole mobility measurements are field and temperature dependant, but are generally found to vary between 10^{-6} and 10^{-7} cm^2/ Vs at 300 K [18-21]. The literature also contains some variation in the HOMO/ LUMO levels. The HOMO levels were agreed to be between 5.1 and 5.2 eV, but the LUMO levels varied between 2.7 – 3.1 eV, resulting in band gap measurements varying from 2.1-2.4 eV [22-26].

The MEH-PPV powder was dissolved in chloroform at concentrations varying from 5 g/ L to 40 g/ L, to obtain a bright orange solution. To avoid coagulation, the solution was mixed in varying stages, usually adding 5 g/ L at a time, and allowing that quantity to dissolve before increasing the concentration. During deposition, the

solution was spread over the sample rather than dropped from above, and the spin coating had to be initiated immediately, to avoid inhomogeneous depositions on account of the highly volatile chloroform. Lower concentrations of MEH-PPV also resulted in more homogeneous depositions, due to reduced viscosity of the solution. The number of polymer coatings varied between one and six layers, with six layers of 10 g/ L MEH-PPV on the ZnO nanowires providing enough resistance to prevent shorts. Once the n-type semiconductor and the quantum dots were added, however, the number of MEH-PPV coatings was reduced to four layers of 10 g/ L.

Once the MEH-PPV was applied, the sample was annealed in vacuum (1 torr) at an initial temperature of 120° C, and allowed to cool back down to room temperature in vacuum. The annealing temperature was initially set to 80° C, but later we found that Alam and Jenekhe used higher annealing temperatures, which may improve the photovoltaic properties by improving the structural order of the MEH-PPV, and increase the mobility of the charge carriers [24].

2.2.3 PEDOT: PSS

Poly(3,4-ethylenedioxythiophene)/poly(styrenesulfonate) (PEDOT:PSS) was used as a hole transport layer in the earliest samples (See Appendix, Table 2). One to two layers were deposited between the MEH-PPV and the Au contact.

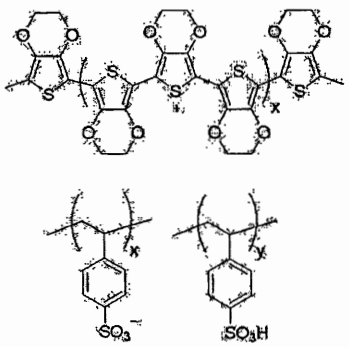

Figure 2.5 Chemical Structure of PEDOT: PSS

Each PEDOT: PSS layer was applied by paintbrush, then baked at ~100° C for 15 minutes. The layer was initially intended to improve hole transport between MEH-PPV and the Au contact, but MEH-PPV itself is a strong hole conductor. The use of PEDOT: PSS was abandoned after Sample 64.

2.3 Milled CdTe

Initially, investigations with quantum dots were done with mechanically milled CdTe obtained from Dr. Uwe Hommerich at Hampton University. Dr. Hommerich used a Spex 800M Mixer/ Mill to mill a sample of 99.99+% pure CdTe powder ($d < 250\mu m$) purchased from Sigma Aldrich. The purpose was to evaluate whether we should purchase a mechanical mill ourselves, in order to produce our own CdTe nanoparticles, or to rely on commercially available quantum dots.

The target particle size was sub-100 nm, so that a CdTe nanoparticle layer would be deposited among the ZnO nanowires, rather than above them. The milled CdTe has two characteristics that make it difficult to use. First, it has a broad size distribution and attempts to filter out the smaller particles were unsuccessful. Second, the particles have a strong tendency to agglomerate, even after high-intensity

sonication. Thus we determined that ligands are a critical component of quantum dots, in order to keep the particles isolated from each other. It was this conclusion that lead to the purchase of the commercial quantum dots from NN-Labs.

2.4 Quantum Dots

2.4.1 Deposition Methods

All of the quantum dot-based solar cells have been prepared by drop coating on the sample a solution of the particles dissolved in either toluene or chloroform and allowing the solvent to evaporate off, either prior to or during annealing. Before the solar cells were fabricated, however, numerous deposition methods were explored, in an attempt to optimize the homogeneity of the coatings. The best method found for obtaining an even layer is spin-coating, but spin-coating wastes too much material to be a feasible deposition method for commercial quantum dots, which are quite expensive.

The various deposition methods investigated include dip coating, painting, and airbrushing solutions of nanoparticles (either TiO_2 or milled CdTe). Dip coating involved repeatedly submerging the substrate in a high concentration solution of the nanoparticles, but the deposited material tended to pool towards the bottom of the sample. Painting the solution on the substrate left brush streaks, visible both in the SEM and by the naked eye. Airbrushing initially appeared to be an ideal deposition method for uniformity, but the force of the air resulted in an uneven spray pattern. The pattern could be avoided by positioning the airbrush further from the sample, but this resulted in a significant amount of wasted material, which, again, would be

impractical for commercial quantum dots. In addition, the degree of homogeneity varied according to the skill of the person using the airbrush, which indicates reproducible results would be difficult to obtain. Drop coating the quantum dots finally became the only viable alternative, but even this method often results in an uneven distribution of material due to differing rates of evaporation on the sample surface.

2.4.2 CdSe Quantum Dots

CdSe is a II-IV compound with a bulk band gap of 1.7 eV, which is well suited to absorbing photons in the solar range. Three vials of CdSe quantum dots were purchased from NN-Labs, with size distributions of 5-10% of the given value.

Parameter	Vial 1	Vial 2	Vial 3
Solvent	Toluene	Toluene	Chloroform
Diameter (nm)	3.4	5.8	5.7
UV Absorption Peak (nm)	565	622	620
Band gap	2.2	2.0	2.0
Concentration (mol/ L)	2.4×10^{-5}	1.3×10^{-5}	1.3×10^{-5}

Table 1 CdSe Quantum Dot Characteristics [39]

The CdSe nanocrystals are coated with octadecylamine ligands that isolate each particle from the others to prevent agglomeration. The CdSe was purchased in a solution comprised of 3.0% CdSe, 97% solvent, and <0.01% ligands. The third vial of

CdSe was dissolved in chloroform, in an attempt to improve the homogeneity of the drop coating deposition by exploiting the quick evaporation of this solvent.

The ligands are insulating and therefore should be removed by annealing. A 420° C anneal was used to activate the CdSe, and the sample was exposed to $CdCl_2$ during the annealing process. Vapors from $CdCl_2$ are often used to slightly p-dope CdTe, and it was incorporated here for the same purpose [25]. The optimal annealing procedures were investigated by varying the parameters slightly for different samples, by either using a vacuum ambient to prevent oxidation or annealing in air to allow better transmission of the $CdCl_2$ vapors to the sample surface. In addition, the time of the anneal was varied from 20 minutes at 430° C, to approximately 2 hours with the oven initially set to 430° C and gradually dropping back down to room temperature.

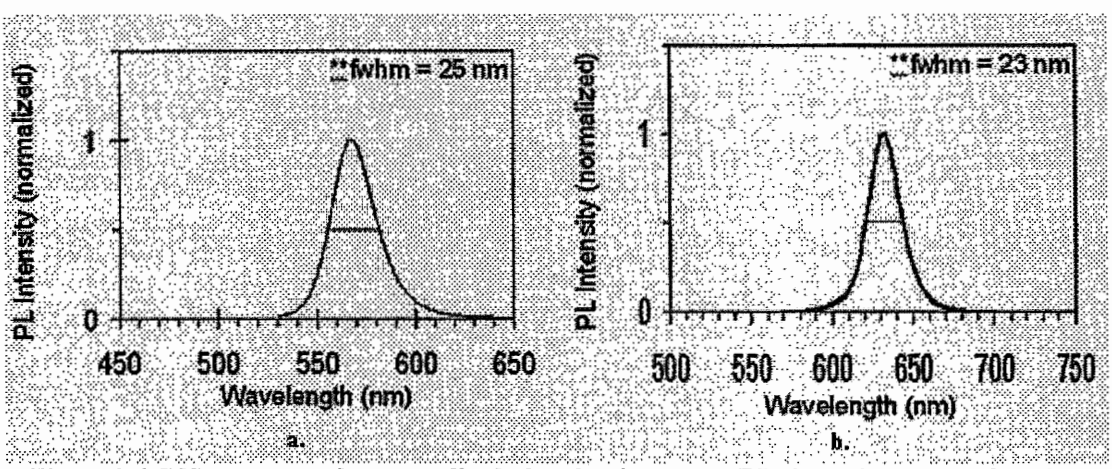

Figure 2.6 CdSe quantum dot normalized photoluminescence (PL) intensity vs. wavelength Fwhm: Full width at half maximum is a measure of the size distribution of a sample [39]. (a.) d=3.4 nm (b.) d=5.7 / 5.8 nm

2.4.3 CdTe Quantum Dots

CdTe is also a II-IV compound, with a bulk bandgap of 1.4 eV which is uniquely suited for optimal absorption in the solar spectrum. One vial of CdTe quantum dots (d = 5.2 nm) in chloroform was custom ordered from NN-Labs. This material had a UV absorption peak of 672 nm (See Figure 2.5) and a concentration of 1.2×10^{-5} mol/ L. Again, the size distribution was within 5-10% of the quoted diameter. The CdTe nanocrystals are coated with octadecylphosphonic acid ligands and purchased in a chloroform solution containing 3.0% CdTe, 97% solvent and <0.01% ligands. The annealing procedures for CdTe were the same as those for CdSe.

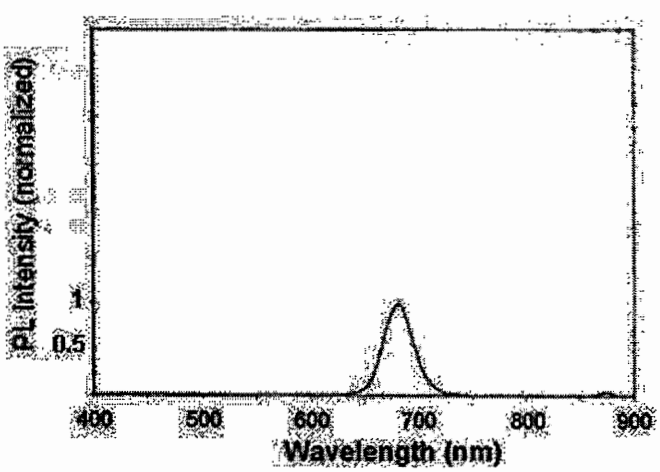

Figure 2.7 CdTe quantum dot normalized photoluminescence intensity vs. wavelength d = 5.2 nm [39]

2.5 Anode Contact

In order to form an ohmic contact at the polymer/ metal interface, it is important that the HOMO level of the p-type polymer match the anode electrode work function [23]. Both the HOMO level of MEH-PPV and the work function of the Au are approximately 5.1 eV.

The gold contact was deposited with a thermal vacuum evaporator that consists of a vacuum chamber ($1x10^{-4}$ torr) with a tungsten wire that can be heated to evaporate gold wire placed upon it. The samples were masked by aluminum foil, and holes were punched in the foil to expose the contact area.

2.6 Sample Characterization

2.6.1 I-V Measurements

Current-voltage (I-V) curves were obtained using a Keithley 236 Source Measure Unit (SMU). The probe measuring the current contacted the gold pad, whereas the probe supplying the voltage contacted an area on the sample scratched down to the FTO substrate and contacted with silver paint. A voltage sweep was applied from –1.0 V to 1.0 V, at 0.1 V increments, with a compliance value set to 1 mA. A delay time of one second allowed the source to settle before the measurement was made and allowed for internal settling on the low current ranges. A default delay is also enabled which is defined according to the selected current range.

I-V measurements were made both when the sample was exposed to light and in the dark. The light source was a 12-V (20 W) incandescent light that illuminated the sample from below. The dark measurements were made with the optical bench covered completely by a black box. The intensity of the white light was equivalent to 0.08 AM1, or 8 mW/ cm^2 and the pad size of the Au contacts was 0.013 cm^2. In most samples, the I-V characteristics were measured for all the pads. In the "Results and Discussion" section, however, only the pad with the best results is presented as representative of the sample's characteristics.

2.6.2 Photovoltage and Photocurrent measurements

Both photovoltage and photocurrent measurements used a Sciencetech 9055 Monochromator with a 115 V 50/ 60 Hz (0.13 A) lamp as the light source. The monochromator has fixed entrance and exit slits, fixed mirrors for focusing, and a rotating diffraction grating. White light is incident on the entrance slit, and reflected onto the diffraction grating. As the grating rotates, a different wavelength is reflected and focused onto the exit slit. A fiber optic cable is attached to the exit slit, and the output is fixed beneath a platform that supports the sample to be measured. A typical wavelength range for solar cell measurement was 350 to 800 nm.

The sample's spectral response was measured by an EG&G 5208 Two Phase Lock-in Analyzer. The lock-in analyzer is capable of detecting the generated photovoltage in the micro-volt range. Light incident on the entrance slit of the monochromator passes through a chopper that operates at a specific frequency. The lock-in amplifier will filter out noise and interference to detect only the signal with the same frequency as the one generated by the chopper.

Initially, photovoltage measurements were the primary tool for determining the spectral response of the earlier samples. The photovoltage measurements were directly output from the EG&G. Eventually, however, photocurrent measurements at short-circuit conditions were necessary for quantum efficiency calculations. A Keithley 428 Current Amplifier was connected to the lock-in amplifier. The current amplifier applies a gain to the photogenerated signal, which is then detected by the lock-in analyzer. The current amplifier is also capable of supplying a voltage to the

probes contacting the sample so that the spectral response can be measured for a range of applied voltages. The photocurrent can then be calculated from the lock-in analyzer data.

The intensity of the monochromator output at the sample was calculated by comparing the typical spectral response of a photodiode to the spectral response output by the lock-in analyzer. The photodiode current output (i (λ)) was measured in response to a wavelength sweep, at 5 nm increments from 300 to 1200 nm. The typical response of the photodiode (Responsivity: R (λ)) was provided in the photodiode specification information. The intensity of the monochromator (I (λ)) is obtained by calculating:

$$I(\lambda) = \frac{i(\lambda)}{R(\lambda)}$$

The intensity was calculated at 5 nm increments, but cell measurements were usually taken at either 10 nm or 20 nm increments.

The energy of the incident photons was calculated from:

$$E_{photon} = \frac{hc}{\lambda_{photon}}$$

Here, h is Planck's constant, c is the speed of light and λ is the wavelength of the incident photon. This information was used along with the I (λ) to calculate the number of incident photons per second:

$$\text{Number of Photons } (\lambda)/\text{ second} = I(\lambda)/ E_{photon}(\lambda)$$

As the lock-in analyzer data was collected for each sample, the same increments were used in order to be able to apply the corrections for each specific wavelength in Excel.

The processing in Excel involved correcting for resistance and the gain that was applied to obtain the photocurrent:

$$\text{Photocurrent (A)} = \frac{\text{EG\&G voltage reading} \times 50\ \Omega}{\text{Applied Gain}}$$

Then the number of electrons generated per second was calculated:

$$\text{Electrons/ second} = \frac{\text{Photocurrent}}{e^-}$$

where e^- is the charge of an electron. From this, the external quantum efficiency was calculated:

$$\text{Quantum Efficiency (\%)} = \frac{\text{Collected electrons}}{\text{Incident photons}} = \frac{\text{Electrons/ second}}{\text{Photons/ second}} \times 100$$

External quantum efficiency vs. wavelength was then plotted for samples with photocurrent measurements.

2.6.3 SEM

An FEI Sirion field emission Scanning Electron Microscope (SEM) was used to investigate the surface quality of the samples. Electron energies from 5 kV to 30 kV were used. The lower accelerating voltages were better for observing organic layer thickness. These layers became more transparent at higher voltages, often revealing details of the ZnO nanowires. The SEM was primarily used for estimating layer thickness, and images were taken both normal to the surface and at angles of 45° to the normal.

3. Results and Discussion

3.1 Cell Design Evolution

Most of the samples were prepared with ZnO nanowires grown on an FTO substrate. The ZnO nanowires enlarge the substrate surface area by approximately a factor of 10, which allows for a reduction of the local thickness of the absorber layer. The morphology of the nanowires assists in the transport of electrons from the center of the active absorber layer to the FTO contact, thereby reducing the length and time necessary for carriers to diffuse. The ZnO nanowires also improve light trapping. Reflecting and refracting the light inside the cell allows the photons to travel further in the material, which increases their probability of absorption [11].

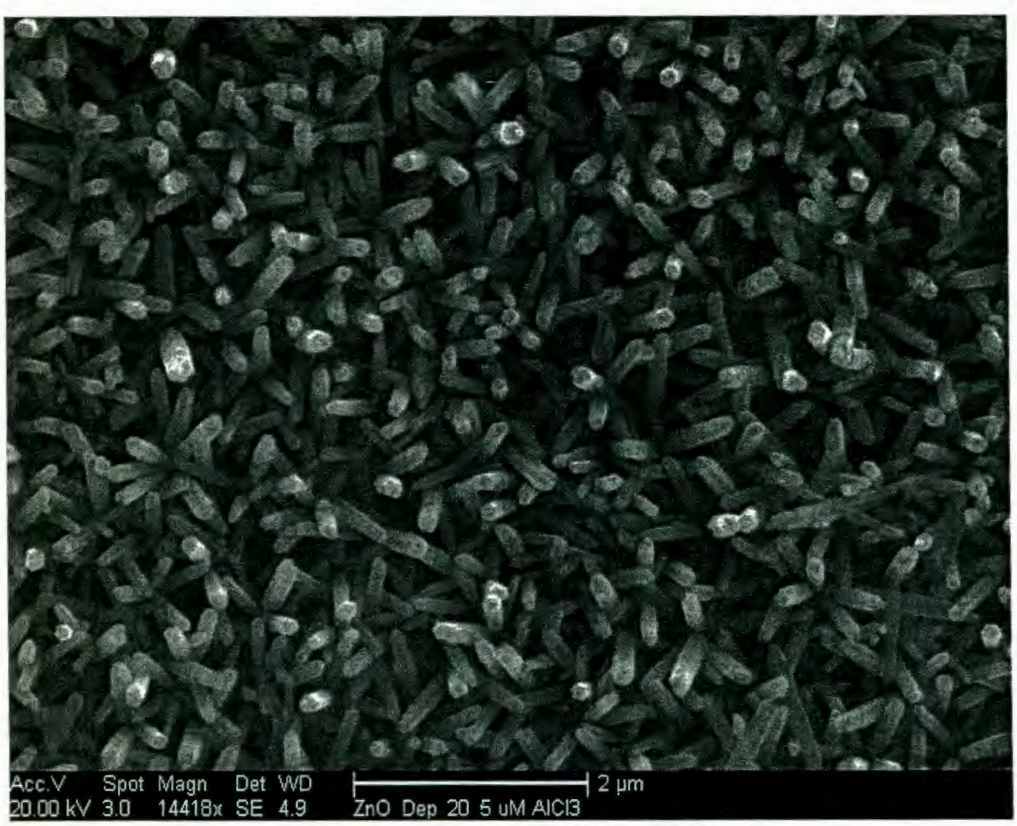

Figure 3.1 ZnO nanowires grown with 5 mM Aluminum

In addition to ZnO nanowires, all of the samples use MEH-PPV as the p-type polymer layer. Prior to combining the organic and inorganic materials, several samples (samples 57-63) were prepared to optimize the layer thickness of MEH-PPV on the ZnO nanowires. The threshold concentration and layer thickness necessary to consistently prevent shorts is six layers of 10 g/ L MEH-PPV in chloroform.

3.1.1 CdTe-based solar cells

Milled CdTe was used as the inorganic absorber layer in samples 69-72 (See Appendix, Table 2). Figure 3.2 is the energy band diagram comparing the work functions, valence-conduction bands, and HOMO/ LUMO levels of the constituent materials.

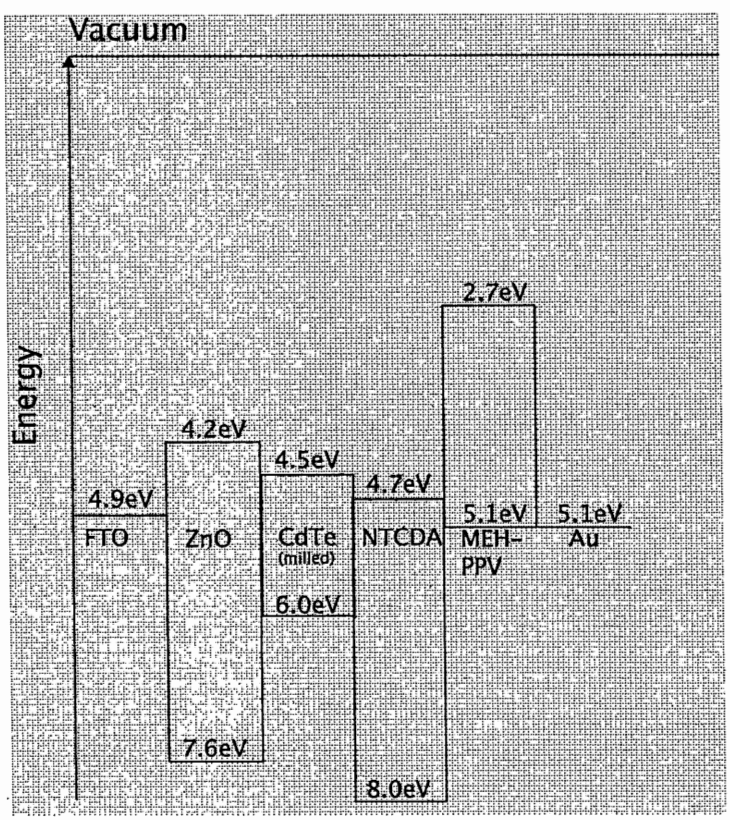

Figure 3.2 Simple energy band diagram for samples with milled CdTe as inorganic absorber layer [13, 27-29].

The first sample (69) was prepared as FTO/ ZnO/ CdTe/ MEH-PPV/ Au. The sample exhibited a strong absorption peak for MEH-PPV (λ_{peak} = 500 nm) (see pg. 17 for MEH-PPV absorption vs. wavelength plot) and a smaller peak for CdTe (λ_{peak} = 835nm).

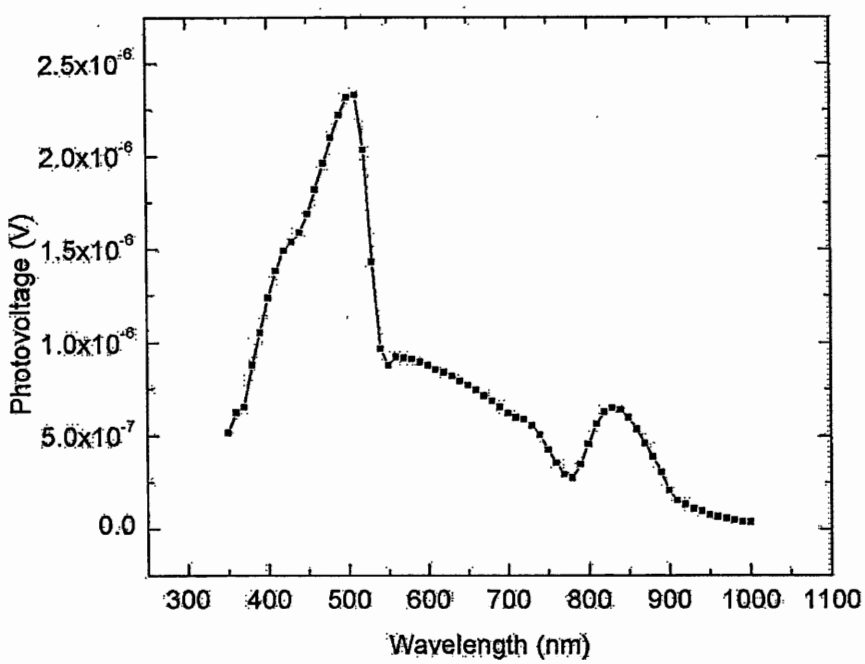

Figure 3.3 Sample 69 Photovoltage.
FTO/ ZnO/ CdTe (milled)/ MEH-PPV/ Au

The next sample included one layer of NTCDA, to provide an n-type layer to improve electron transport from CdTe to the ZnO nanowires. In addition, this layer was added to form a p-n junction with the MEH-PPV, to obtain rectification in the I-V curves. The NTCDA was deposited after the CdTe to layer the materials according to decreasing annealing temperatures.

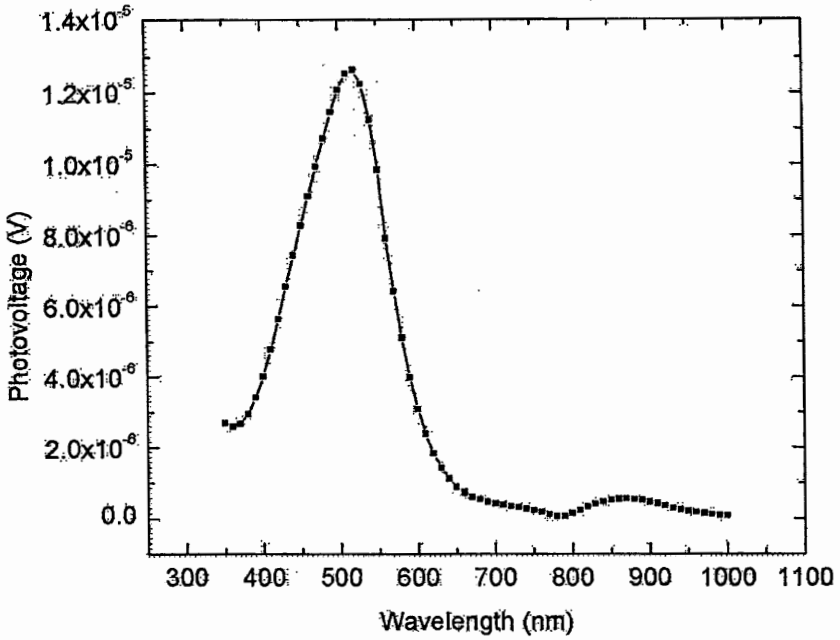

Figure 3.4 Sample 71 Photovoltage.
FTO/ ZnO/ CdTe (milled)/ NTCDA/ MEH-PPV/ Au

In comparison to Sample 69 (Figure 3.3), the addition of NTCDA in Sample 71 improved the photovoltage due to MEH-PPV by almost an order of magnitude and I-V characteristics indicated excellent rectification. Photovoltage attributed to CdTe, however, was smaller. The decrease in CdTe response may have been due to the sequence of the layers. Holes generated by the CdTe may not be transported through the NTCDA on their way to the MEH-PPV. Some samples incorporating CdSe were also prepared according to this scheme.

Sample 72 is similar to Sample 69, without the ZnO nanowires. For Sample 72 (Figure 3.5), MEH-PPV absorption was the same and CdTe absorption was stronger, compared to Sample 69 (Figure 3.3).

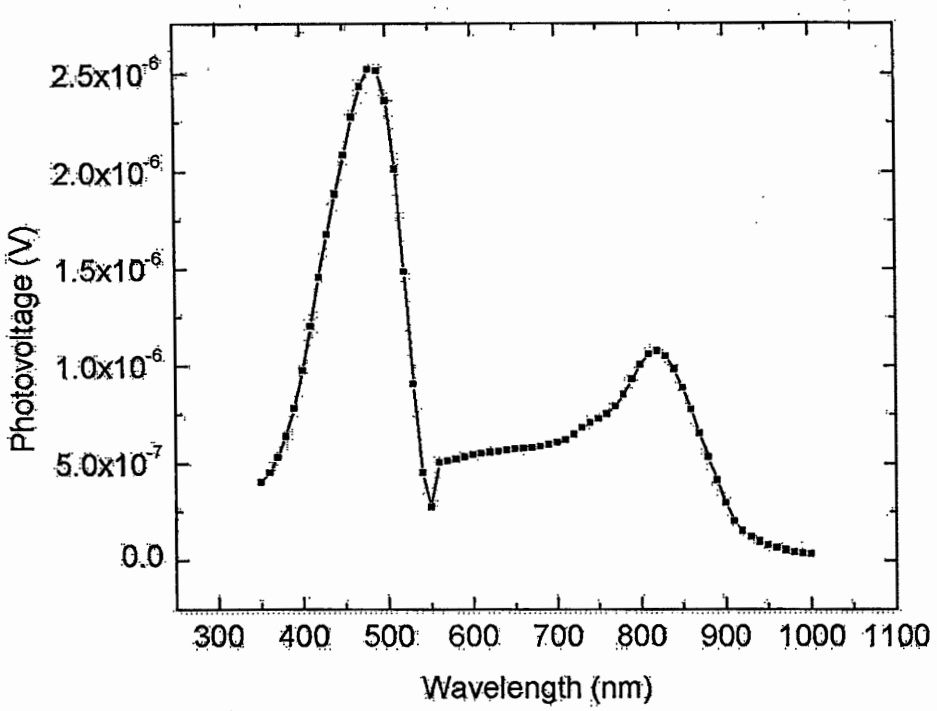

Figure 3.5 Sample 72 Photovoltage
FTO/ CdTe (milled)/ MEH-PPV/ Au

SEM images of Sample 69 also showed a very thick layer (~22 μm) of the milled CdTe particles. In Figure 3.6, the surface of Sample 69 was scratched, to obtain a thickness estimate of the milled CdTe particle layer. The CdTe layer is thick enough to obscure the ZnO nanowires. Both the reduced photovoltage peak of milled CdTe on the ZnO nanowires (Figure 3.5 vs. Figure 3.4) and the thickness of the CdTe layer (Figure 3.6) suggest poor contact between CdTe particles and the nanowires. The design therefore does not exploit the potential advantages offered by the increased surface area of the nanowires. We therefore decided not to use milled CdTe as the inorganic absorber layer.

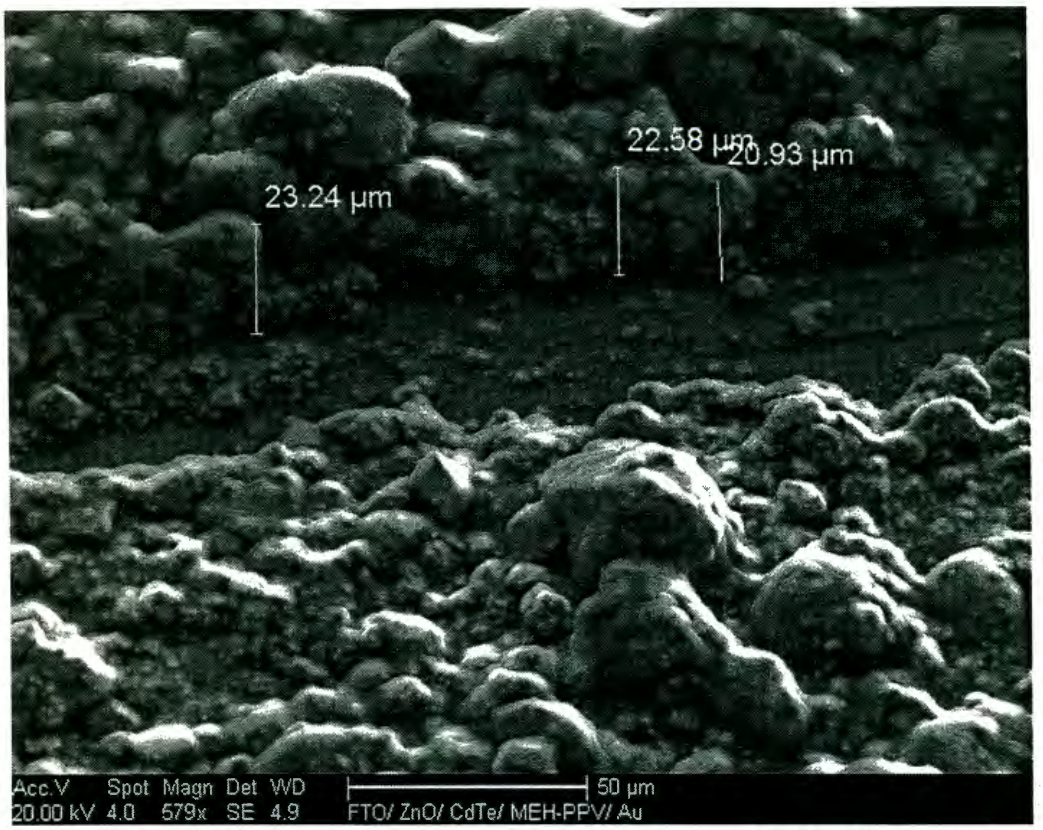

Figure 3.6 SEM image of milled CdTe on ZnO with six layers MEH-PPV (Sample 69)

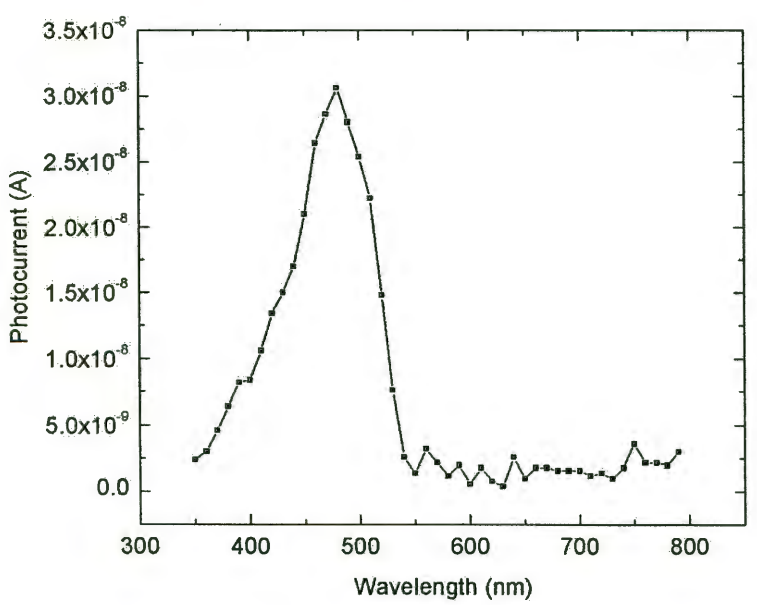

Figure 3.7 Sample 85 Photocurrent
FTO/ Al-doped ZnO/ NTCDA/ CdTe (d= 5.2nm)/ MEH-PPV/ Au

We turned instead to CdTe quantum dots custom ordered from NN-Labs. Samples prepared with CdTe quantum dots, however, did not exhibit any absorption in the expected wavelength range (λ_{peak} = 672 for d = 5.2 nm), as shown in Figure 3.7 on the previous page. This result may be due to unfavorable energy offsets that are indicated in the adjusted energy band diagram in Figure 3.8.

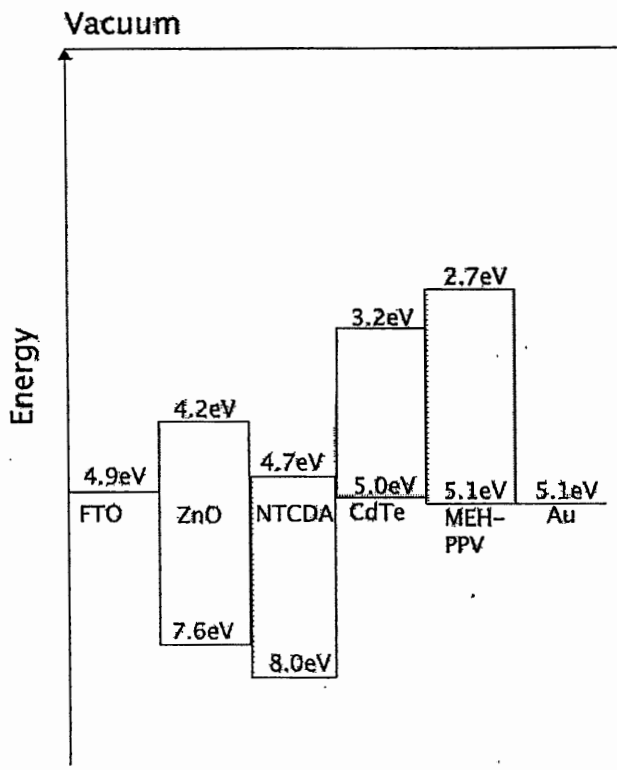

Figure 3.8 Simple energy band diagram for samples with CdTe quantum dots (d = 5.2 nm) as the absorber layer [13, 27, 28, 30].

The band gap increase that occurs as a particle approaches the molecular scale shifts the energy levels and, once in the quantum dot size range, the LUMO level tends to increase as the particle sizes decrease (See Figure 1.4). The band diagram in Figure 3.8 shows that the CdTe quantum dots have a lower conduction band and higher valence band in comparison to the LUMO/ HOMO levels of MEH-PPV. This

suggests that, although energy transfer is favorable from MEH-PPV to CdTe, electron and hole transfer from the CdTe to the MEH-PPV would be blocked by the level mismatch [8, 30].

3.1.2 CdSe-based solar cells

CdSe quantum dots were used next. The samples incorporating CdSe quantum dots as the absorber layer exhibited the most promising results. The energy band diagram is shown in Figure 3.9.

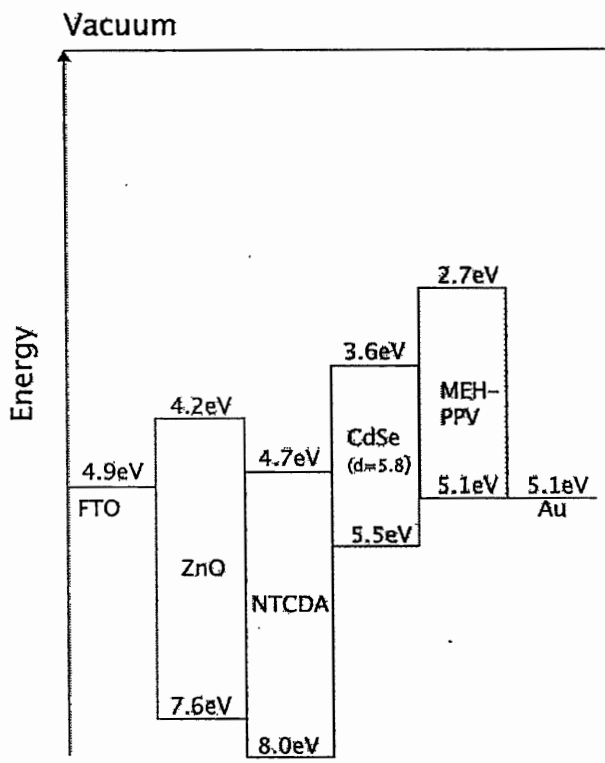

Figure 3.9 Simple energy band diagram for samples with CdSe quantum dot absorber layer [13, 27, 28, 31].

The diagram in Figure 3.9 is designed for the CdSe quantum dots (d=5.8 nm) with λ_{peak} = 620 nm, but can be interpreted for λ_{peak} = 565 nm (d=3.4 nm) by shifting the LUMO level up by 0.2 eV to 3.4 eV [8, 30].

A slight modification in the measuring procedures can be observed in the following samples. As mentioned in the experimental section, a current amplifier was connected to the lock-in analyzer, in order to measure photocurrent rather than photovoltage. The quantum efficiency was then calculated from the photocurrent measurements (See Section 2.6.2).

Sample 78 was prepared with the original layering scheme, with NTCDA following the CdSe deposition (See Figure 3.10, pg. 36). Absorption due to both MEH-PPV (λ_{peak} = 500 nm) and CdSe (λ_{peak} = 565 nm) are evident in this spectrum. This was the first sample to incorporate ZnO nanowires grown with 5 μM $AlCl_3$ in the standard deposition solution (See Section 2.1), to improve the electrical characteristics of the ZnO by increasing the electron density in the nanowires [11]. CdSe was annealed at an initial temperature of 430° C in air while exposed to $CdCl_2$. The dry $CdCl_2$ powder was sprinkled inside an aluminum foil box that enclosed the sample during the anneal. One layer of 10 g/L NTCDA was annealed in vacuum at an initial temperature of 300° C, followed by six layers of 10 g/ L MEH-PPV annealed in vacuum at an initial temperature of 125° C. Each anneal involved setting the initial temperature, and allowing the annealing oven to drop back down to room temperature in vacuum.

In Figure 3.11, the I-V characteristics showed a pronounced difference between measurements taken under exposure to light, and those measured in the dark (For all I-V measurements, white light source is I = 8 mW/ cm^2, Au contact area is 0.013cm^2).

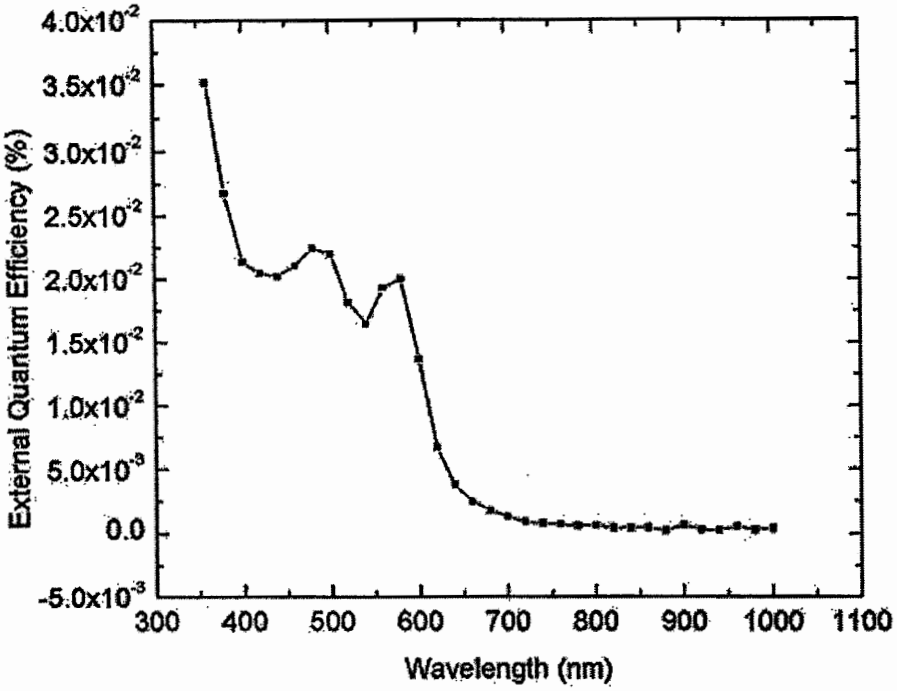

Figure 3.10 Sample 78 External quantum efficiency
FTO/ Al-doped ZnO/ CdSe (d = 3.4 nm)/ NTCDA/ MEH-PPV/ Au

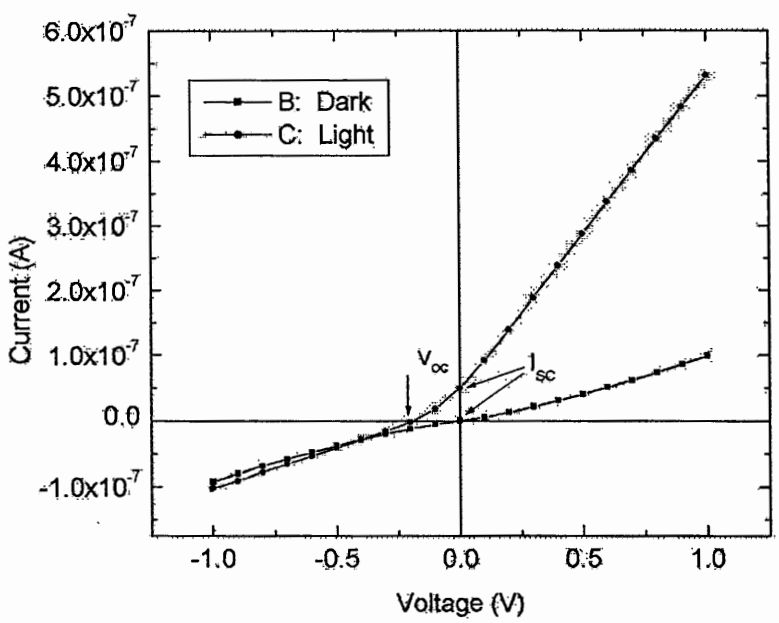

Figure 3.11 Sample 78 I-V Curve
FTO/ Al-doped ZnO/ CdSe (d = 3.4 nm)/ NTCDA/ MEH-PPV/ Au

In the I-V curve, the open circuit voltage (V_{oc}) is measured as the voltage offset between where the photocurrent and the current measured in the dark cross the I = 0 axis. The short circuit current (I_{sc}) is the difference between where the two curves cross V = 0. As indicated in Figure 3.11, V_{oc} = -0.2 V and $I_{sc} = 5 \times 10^{-8}$. The voltage is supplied to the FTO substrate, while the current is collected at the Au pad. Since V_{oc} is negative and I_{sc} is positive, the photocurrent is conducted in the expected direction, with the electrons moving to the FTO via the ZnO nanowires, while the holes are transported to the Au top contact.

Sample 79 was prepared with all of the same materials and processing procedures as 78, but without the ZnO nanowires (See Figure 3.12, pg. 39). The magnitude of the efficiency peaks due to MEH-PPV and CdSe are higher without the ZnO nanowires (Figures 3.10 vs. 3.12). The I-V curve for Sample 79 has a larger V_{oc} at –0.4 V than Sample 78, whereas the current is reduced to 3×10^{-8} A (See Figure 3.13, pg. 39).

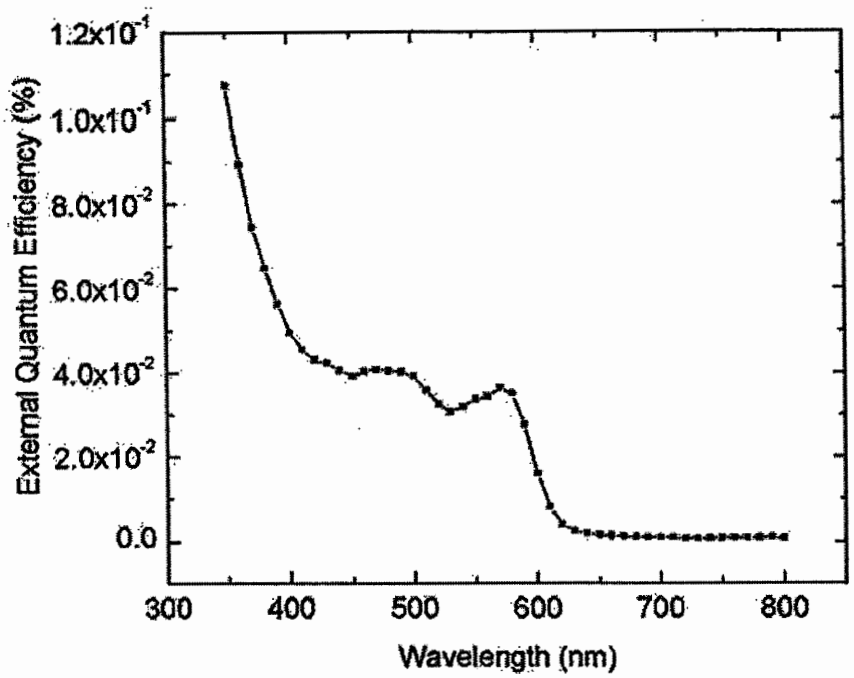

Figure 3.12 Sample 79 External quantum efficiency
FTO/ CdSe (d-3.4 nm)/ NTCDA/ MEH-PPV/ Au

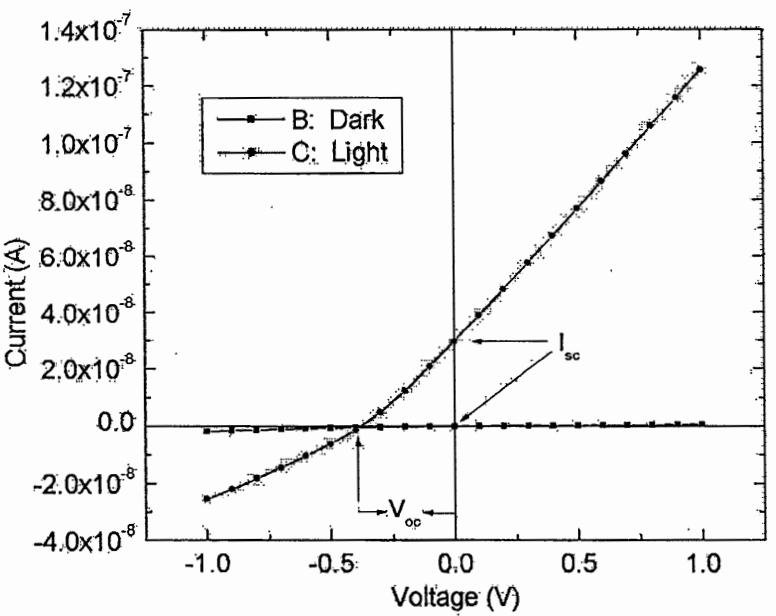

Figure 3.13 Sample 79 I-V characteristics
FTO/ CdSe (d-3.4 nm)/ NTCDA/ MEH-PPV/ Au

At this point, we re-evaluated the layer sequence. In samples prepared after 79, the NTCDA was deposited prior to the CdSe quantum dot deposition in order to provide an n-type layer to assist in transporting electrons through the nanowires and also to allow the holes to reach the MEH-PPV layer prior to recombination. This is the layering scheme proposed in the Figure 3.9 band diagram (pg. 35). Although this approach seems favorable with respect to the HOMO/ LUMO energy offsets, there is still concern regarding the temperature necessary for the CdSe anneal, and the effects this may have on the NTCDA. Although the NTCDA specifications state that this material has a melting point greater than 300° C, they do not specify the precise temperature, and the 430° C anneal necessary for CdSe is substantially higher than 300° C.

To investigate the effect of this high temperature anneal, NTCDA was deposited on an FTO-coated glass substrate. First, the resistance of the bare FTO was measured to be 18.2 Ω at two designated positions on the substrate. Then a layer of 10 g/ L NTCDA was deposited on the FTO and the resistance was measured at the same positions to be 19.2 Ω. The sample was annealed in air at 430° C, and remained in the annealing oven until the temperature dropped back down to room temperature, as is the standard procedure for the CdSe anneal. The resistance of the sample was measured to be 19.4 Ω after the 430° C anneal. Although this simple experiment does not verify the molecular integrity of the NTCDA, it does confirm that the layer did not evaporate off during the high temperature anneal.

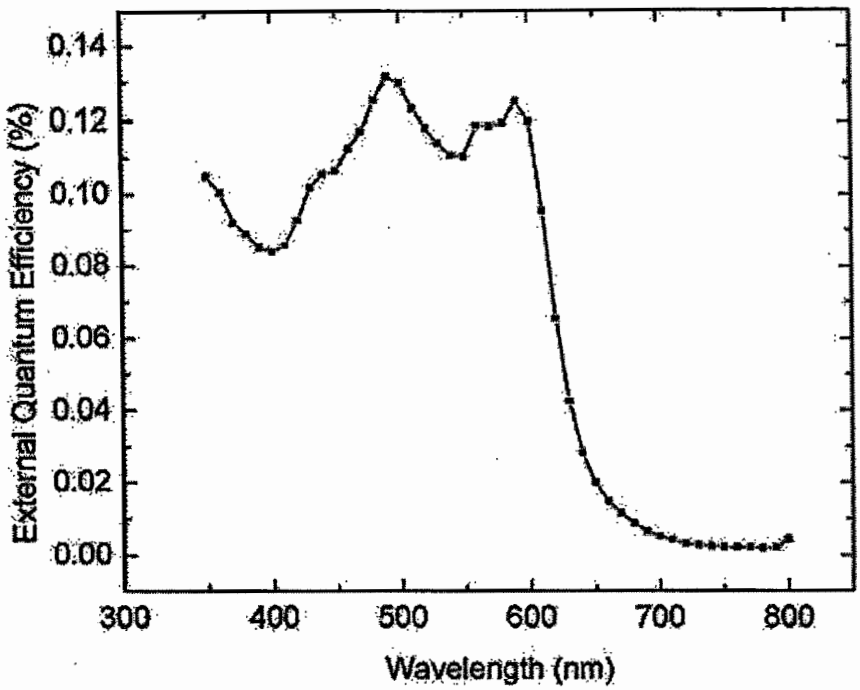

Figure 3.14 Sample 81 External quantum efficiency
FTO/ Al-doped ZnO/ NTCDA/ CdSe (d=5.8nm)/ MEH-PPV/ Au

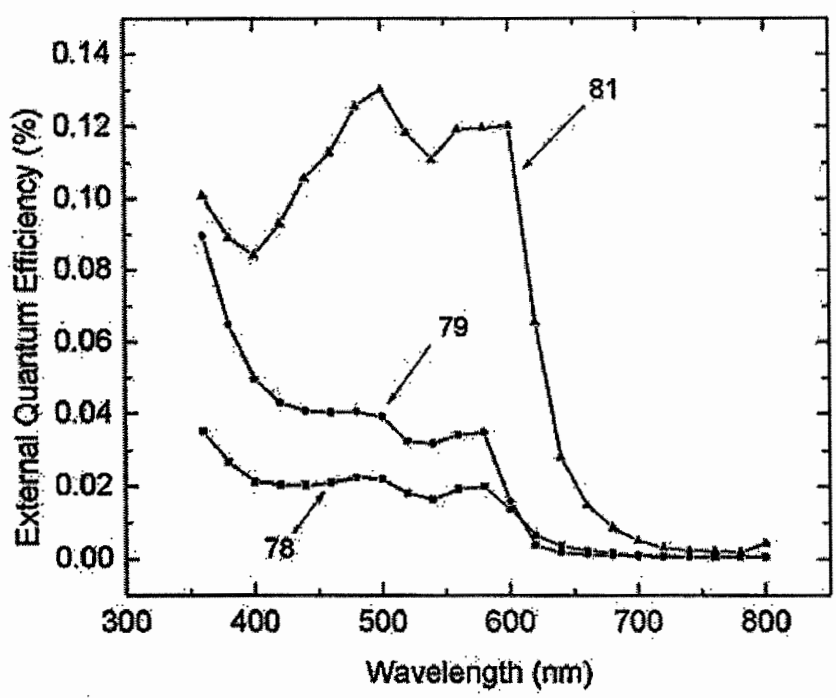

Figure 3.15 Comparison of Samples 78, 79 and 81

Sample 81 was the first sample prepared with the NTCDA layer before the deposition of the CdSe quantum dots. One layer of 10 g/ L NTCDA and six layers of 10 g/ L MEH-PPV were deposited (See Figure 3.14, pg. 41). Sample 81 was prepared with the annealing temperatures and procedures addressed above for samples 78 and 79.

In comparing Sample 81 to 78 and 79, both the peaks attributed to MEH-PPV and CdSe are higher by a factor of 6 and 3, respectively (See Figure 3.15, Pg. 41). In addition, the range of wavelengths absorbed was extended by using the CdSe quantum dots with d = 5.8 nm, rather than the CdSe particles with d = 3.4 nm that were used in samples 78 and 79.

In comparing the curves for the CdSe particles with different diameters, there may have been efficiency losses in samples 78 and 79 due to competition for absorption of photons in the same wavelength range by both MEH-PPV (λ_{peak} = 500 nm) and CdSe with d = 3.4 nm (λ_{peak} = 565 nm). The success of Sample 81 relative to the others prompted the purchase of more CdSe quantum dots, with d = 5.8 nm (λ_{peak} = 620 nm).

The I-V curves of Sample 81 exhibited slight rectification, but both the short circuit current and the open circuit voltage improved, at $I_{sc} = 2 \times 10^{-7}$ and $V_{oc} = -0.45$ V (See Figure 3.16, pg. 43). The improvement in the open circuit current is an order of magnitude higher than that of Samples 78 and 79, which confirms the advantage of layering the NTCDA before the CdSe, as opposed to after.

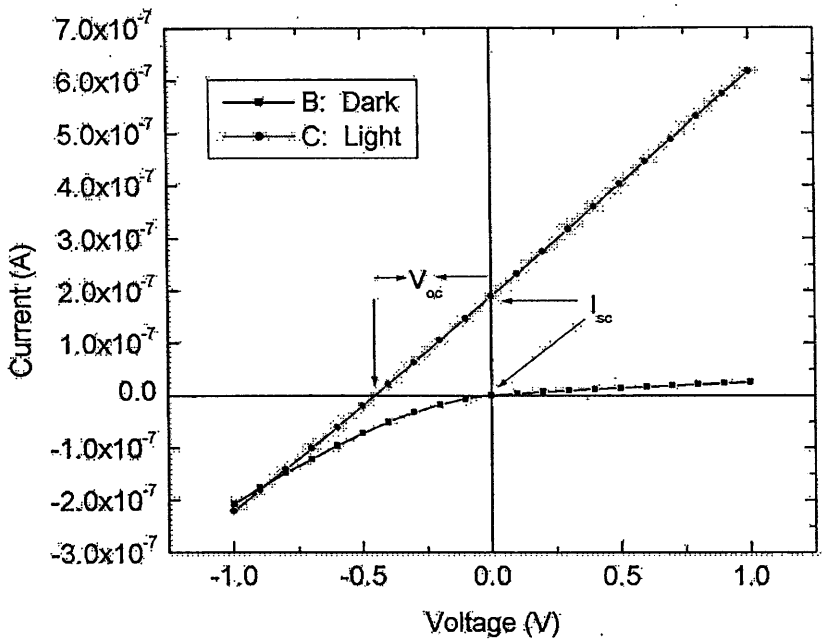

Figure 3.16 Sample 81 I-V characteristics
FTO/ Al-doped ZnO/ NTCDA/ CdSe (d = 5.8nm)/ MEH-PPV/ Au

The concentration of NTCDA was reduced to 3 g/ L (as opposed to 10 g/ L) to minimize the thickness of the electron transport material between the CdSe absorber layer and the ZnO nanowires. The NTCDA layer was incorporated to improve the p-n junction and to act as a wetting layer, thereby permitting motion of the charge carriers in the regions between the quantum dots. The 3 g/ L NTCDA layer is transparent in the SEM image in Figure 3.17 (pg. 44), because the accelerating voltage is at 20 keV and the electron beam is normal to the sample surface. The layer can, however, be observed in Figure 3.18 (pg. 44) as the thin coating obscuring the morphology of the ZnO nanowires. In Figure 3.18, the platform supporting the sample is at a 45°, and the accelerating voltage has been reduced to 10 keV.

Figure 3.17 One layer 3 g/ L NTCDA on ZnO, 20 keV

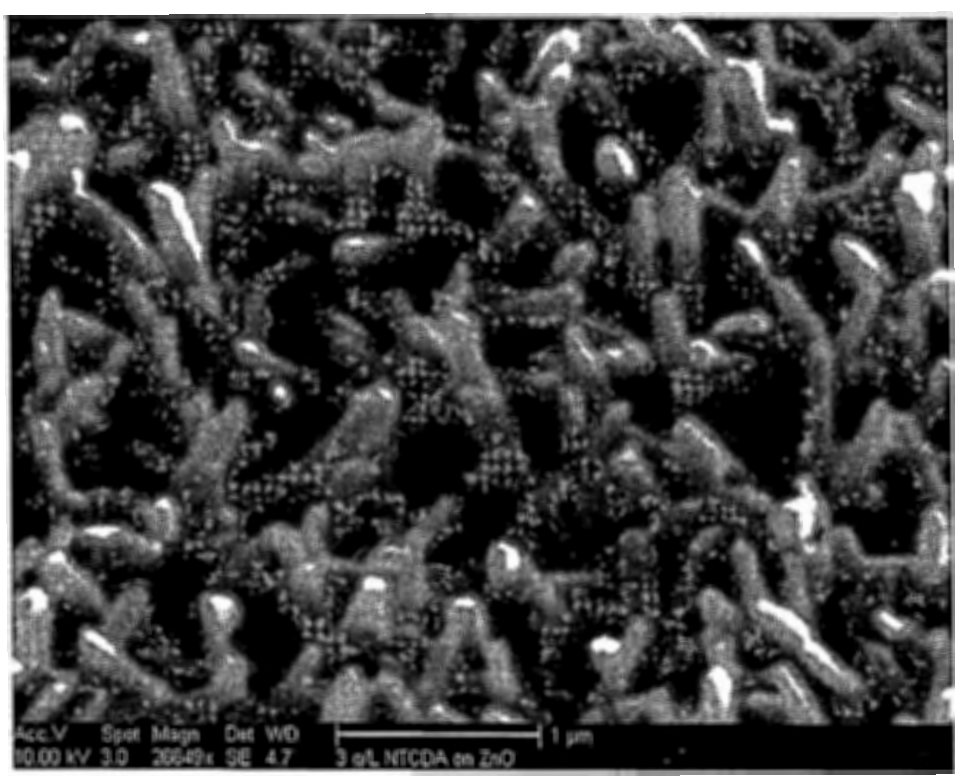

Figure 3.18 One layer 3 g/ L NTCDA on ZnO, 10 keV at 45°

Sample 84 was the first sample prepared with a layer of 3 g/ L NTCDA, instead of 10 g/ L (See Figure 3.19 below). In addition, the number of MEH-PPV coatings was reduced to four layers of the 10 g/ L solution. Although the threshold thickness of MEH-PPV necessary to prevent electrical shorts had previously been determined to be six layers, the experiments to determine the threshold thickness had been conducted using MEH-PPV along with a single layer of PEDOT-PSS, whereas the samples being prepared at this point have both the NTCDA and the CdSe quantum dot materials present. It appears plausible that the increase in resistance provided by these additional materials could allow for a reduction in the necessary MEH-PPV layer thickness.

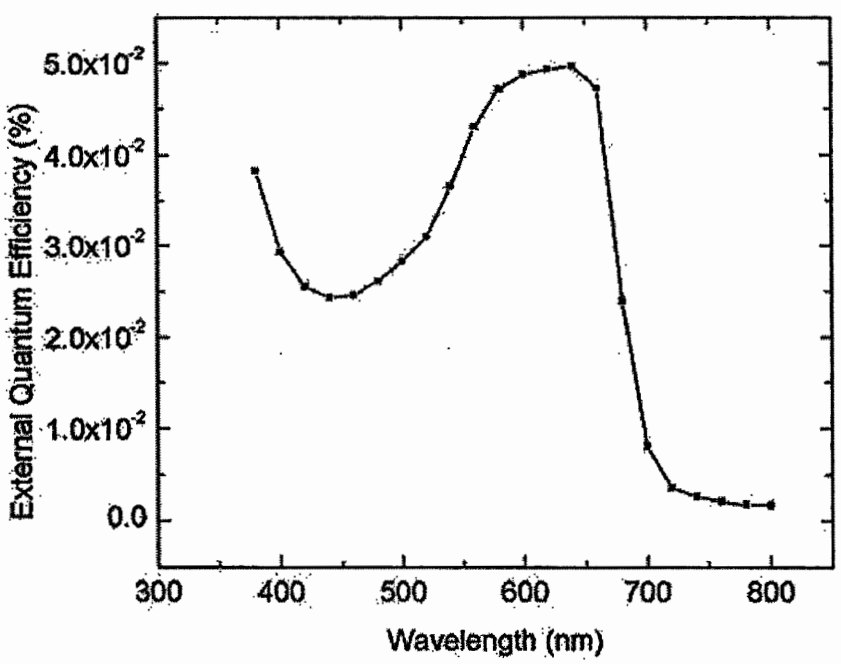

Figure 3.19 Sample 84 External quantum efficiency
FTO/ Al-doped ZnO/ NTCDA (3 g/ L)/ CdSe (d = 5.8nm)/ MEH-PPV (4 layers, 10 g/ L)/ Au

The annealing procedures for Sample 84 were also different from previous samples. Rather than setting the initial temperature, and allowing the oven to drop back down to room temperature, both the MEH-PPV and the CdSe were annealed at sustained temperatures of 420° C for 20 minutes in air and 125° C for 8 hour in vacuum, respectively. For both anneals, the sample was removed at the elevated temperature.

We determined that four layers of 10 g/ L MEH-PPV, in combination with the NTCDA and CdSe, were thick enough to prevent shorts. As is evident in Figure 3.19 (pg. 45), the predicted CdSe absorption peak at 620 nm is broader than before and there is no distinctive MEH-PPV peak. The MEH-PPV absorption, however, may be encompassed in the wider, single peak that tapers down past the 500 nm range and is also evident in the UV. The efficiency for sample 84 is less than that of Sample 81, but the CdSe peak is higher than that observed for both Samples 78 and 79.

It is possible that the modified annealing procedures may have damaged the conductive compounds in this sample. By removing the sample at an elevated temperature, there is a higher risk for oxidation. In later samples, as before, the samples were removed at room temperature.

Sample 86 was designed to investigate alternative annealing procedures for the CdSe quantum dots. In order to prevent the possibility of damage to the NTCDA at the 430° C anneal, the CdSe was deposited immediately after one layer of 10 g/ L NTCDA and both materials were annealed at 300° C in vacuum, without the $CdCl_2$. Then four layers of 10 g/ L MEH-PPV were deposited and annealed in vacuum using

the original procedure of setting the temperature at 125° C and allowing the oven to drop back down to room temperature in vacuum.

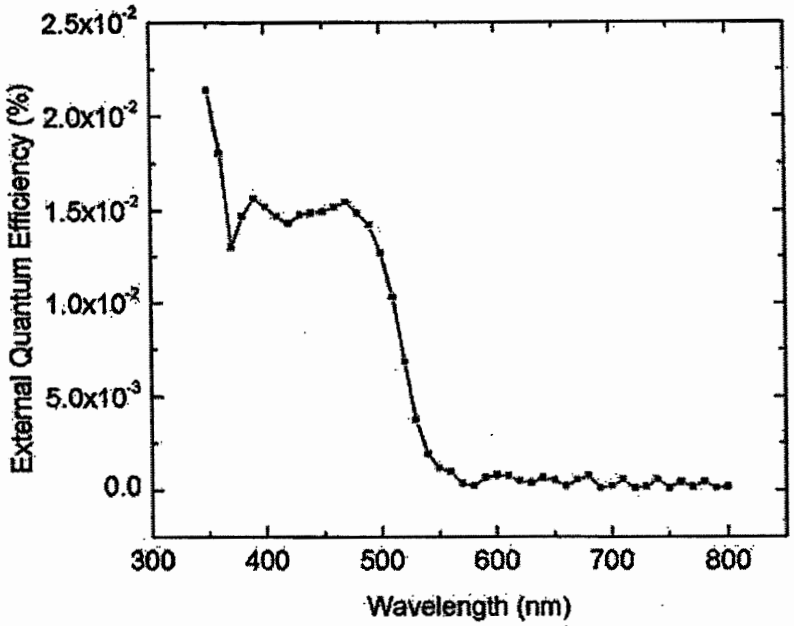

Figure 3.20 Sample 86 External quantum efficiency
FTO/ Al-doped ZnO/ NTCDA/ CdSe (d = 5.8 nm)/ MEH-PPV: No CdSe Anneal

Clearly, there is no CdSe absorption peak. The octadecylamine ligands surrounding the CdSe quantum dots have a melting point of 55 to 57° C, and thus must be removed in the annealing [32]. It is therefore assumed that the CdSe needs the 430° C anneal, in order to improve the electronic properties of the quantum dots.

In sample 92, sample 81 was prepared again, but without NTCDA (See Figure 3.21, pg. 48). Thus the CdSe was layered directly on the Al-doped ZnO nanowires and annealed in air at an initial temperature of 430° C with $CdCl_2$. This was followed by six layers of 10 g/ L MEH-PPV annealed at an initial temperature of 125° C in vacuum. Both annealing procedures followed the original process of allowing the oven to drop down from the initial temperature back to room temperature in vacuum.

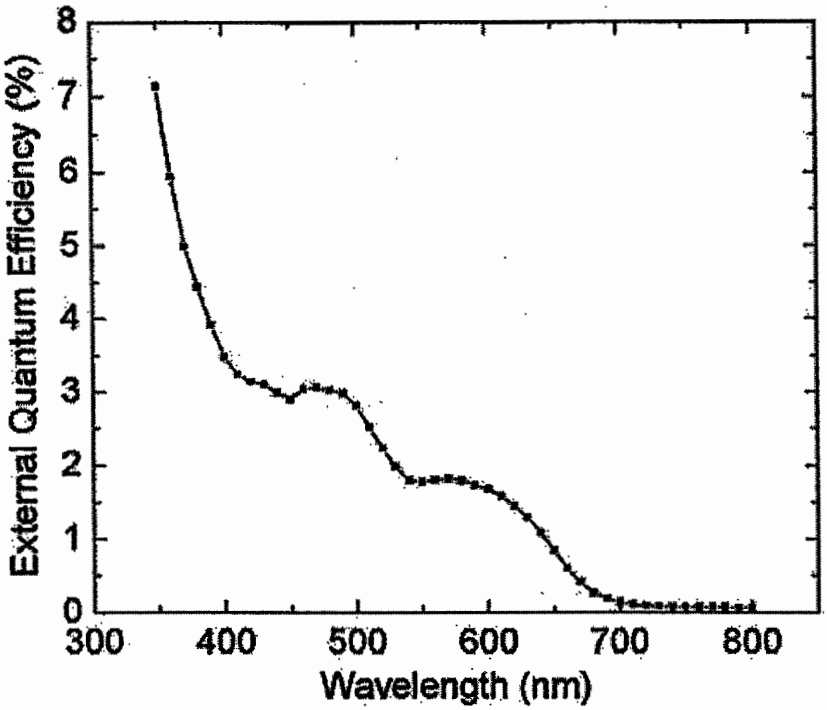

Figure 3.21 Sample 92 External quantum efficiency
FTO/ Al-doped ZnO/ CdSe (d = 5.7 nm)/ MEH-PPV/ Au: No NTCDA

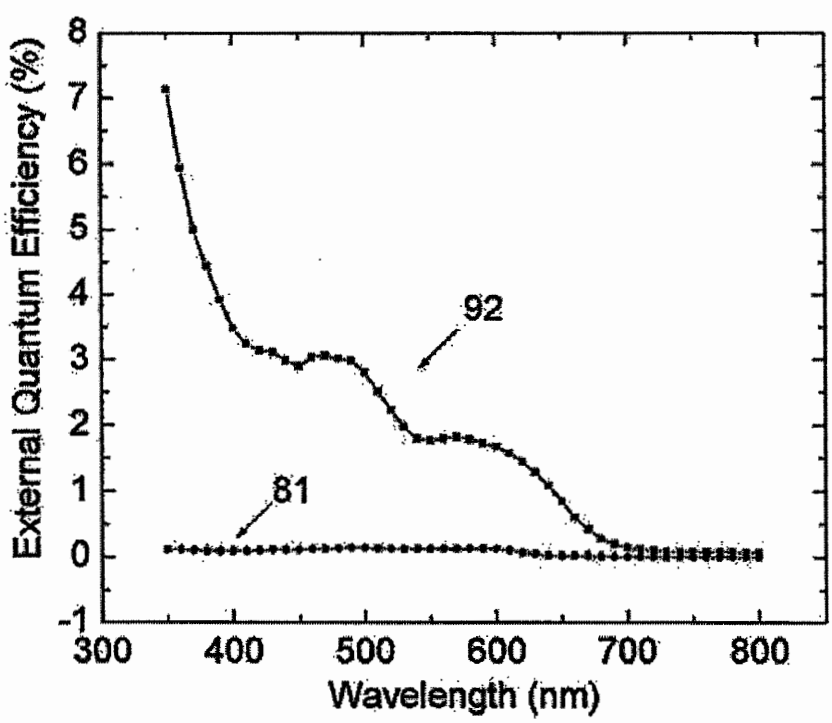

Figure 3.22 Comparison of Samples 81 and 92

Sample 92 suggests that the NTCDA layer has a detrimental effect on the sample efficiency, possibly due to the NTCDA LUMO level that lies below the ZnO conduction band (See Figure 3.9).

The I-V characteristics for sample 92 (Figure 3.23 below) do not indicate rectification, but $I_{sc} = 1.15 \times 10^{-6}$ A, which is almost an order of magnitude higher than that of Sample 81. The V_{oc} is slightly smaller at –0.2 V. The improved photocurrent is probably due to the favorable band offsets in the energy band diagrams in Figure 3.9, without the NTCDA. This design allows the cell to exploit both the electron transport properties and the increased surface area of the ZnO nanowires. The removal of the n-type layer may also, however, lower V_{oc} and reduce rectification due to a less pronounced p-n junction.

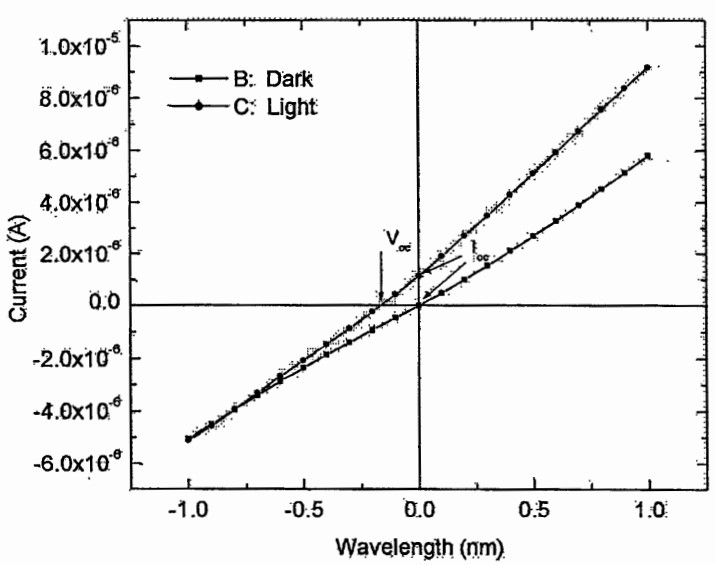

Figure 3.23 Sample 92 I-V characteristics
FTO/ Al-doped ZnO/ CdSe (d = 5.7 nm)/ MEH-PPV/ Au: No NTCDA

Sample 92 was similar to sample 64 (See Figure 3.25, pg. 51), which was prepared early in this project. Sample 64, however, had a layer of PEDOT-PSS between the MEH-PPV and the gold contact layer (See Figure 3.24 below). Out of nine pads on the sample, four failed to exhibit a photovoltage response, and the magnitude of those photovoltage peaks were low, compared to previous samples. This may have been due to electrical shorts and poor overall conductivity of the sample. To compare the two, we measured the photovoltage of Sample 92, since efficiency measurements of the older sample would be unreliable after so much time since fabrication. Figure 3.26 (pg. 51) clearly shows the improved photovoltage response in Sample 92, as compared to 64.

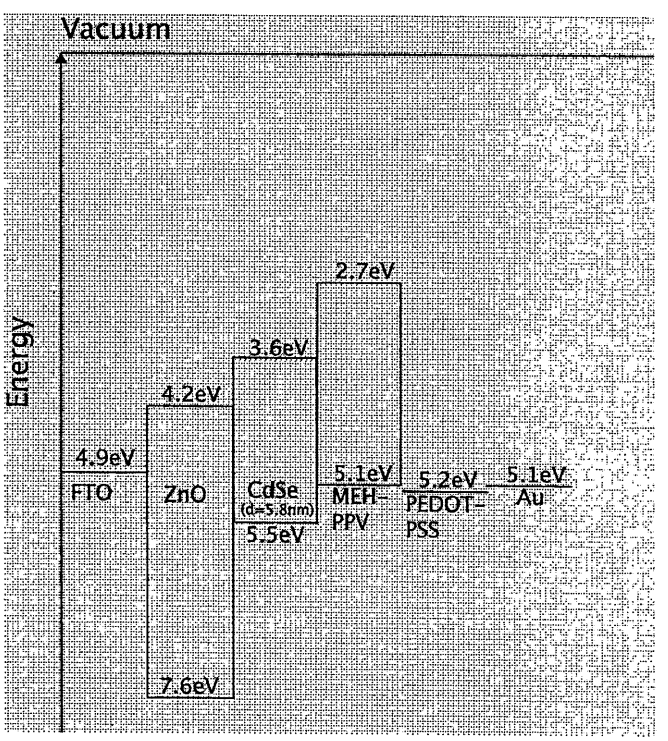

Figure 3.24 Energy band diagram for Sample 64

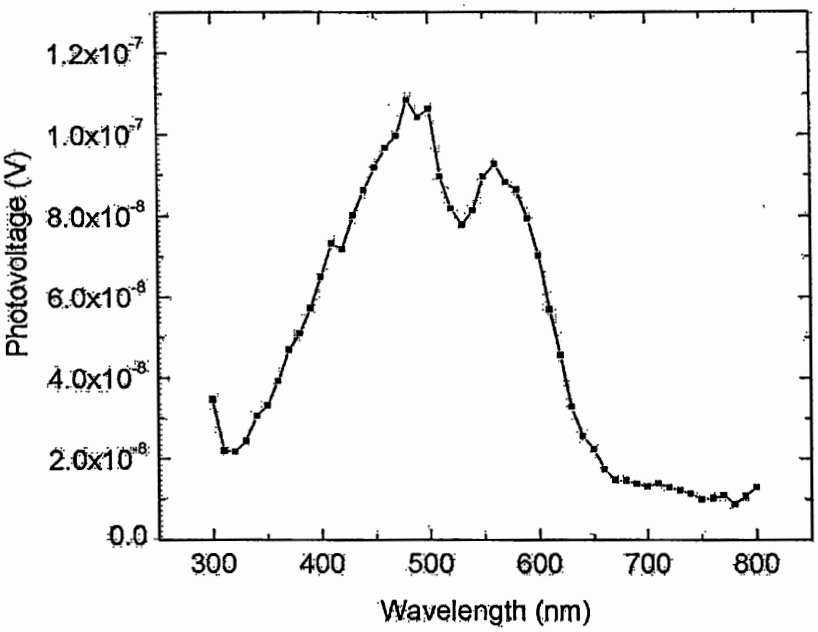

Figure 3.25 Sample 64 Photovoltage
FTO/ ZnO/ CdSe (d = 3.4 nm)/ MEH-PPV/ PEDOT-PSS/ Au

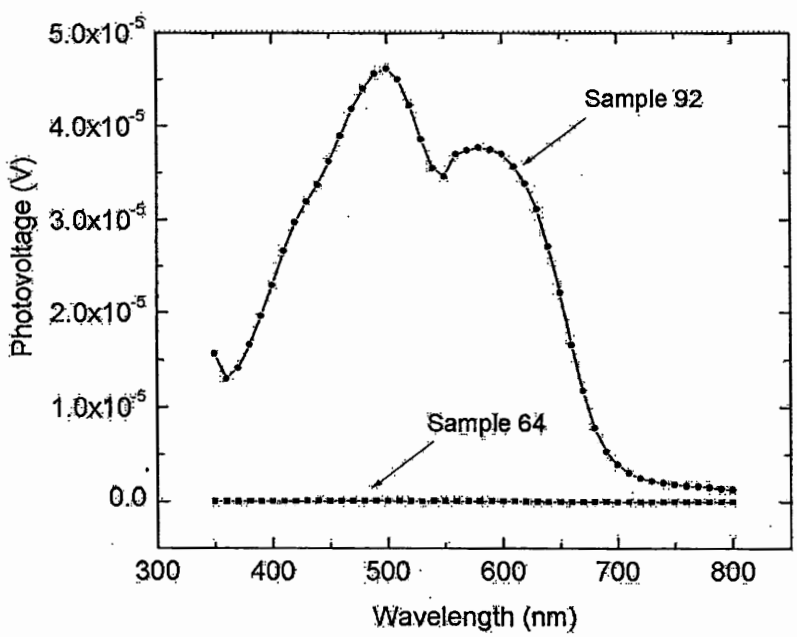

Figure 3.26 Comparison of Samples 64 and 92

Sample 93 was prepared to determine the influence of the ZnO nanowires on the efficiency of Sample 92. Sample 93 was prepared with the same materials and procedures as 92, without the ZnO nanowires (See Figure 3.27 below). The CdSe was deposited on FTO and annealed in air at an initial temperature of 430° C with $CdCl_2$. This was followed by six layers of 10 g/ L MEH-PPV annealed at an initial temperature of 125° C in vacuum. Both annealing procedures followed the original process of allowing the oven to drop down from the initial temperature back to room temperature in vacuum.

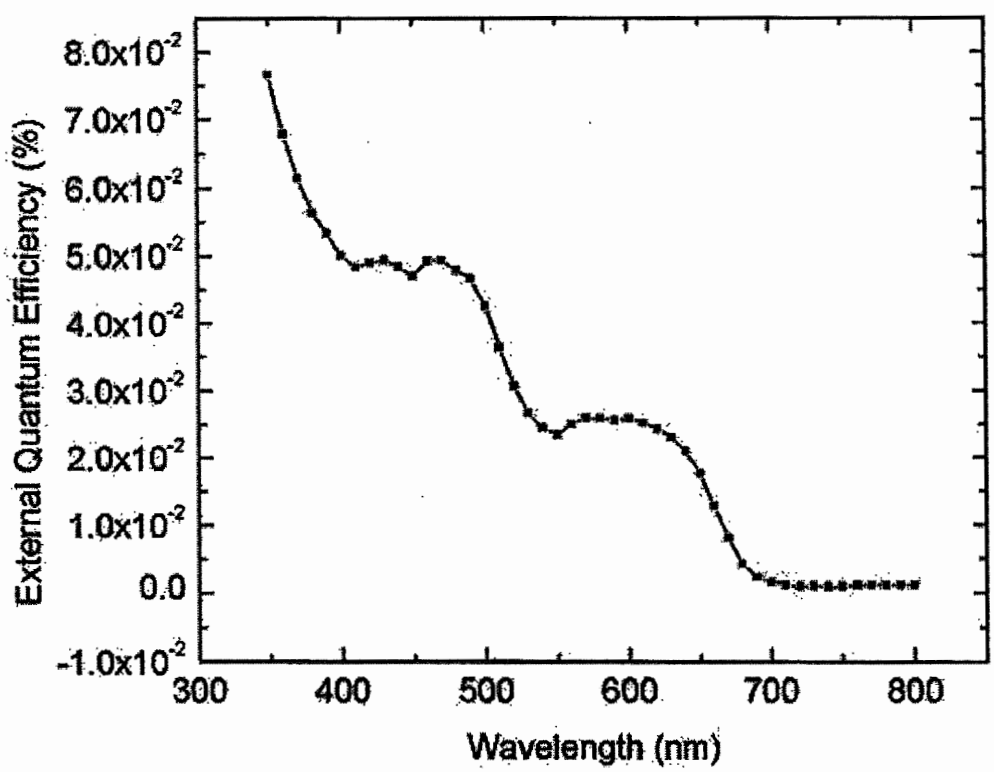

Figure 3.27 Sample 93 External quantum efficiency
FTO/ CdSe (d = 5.7 nm)/ MEH-PPV/ Au: No NTCDA, No ZnO

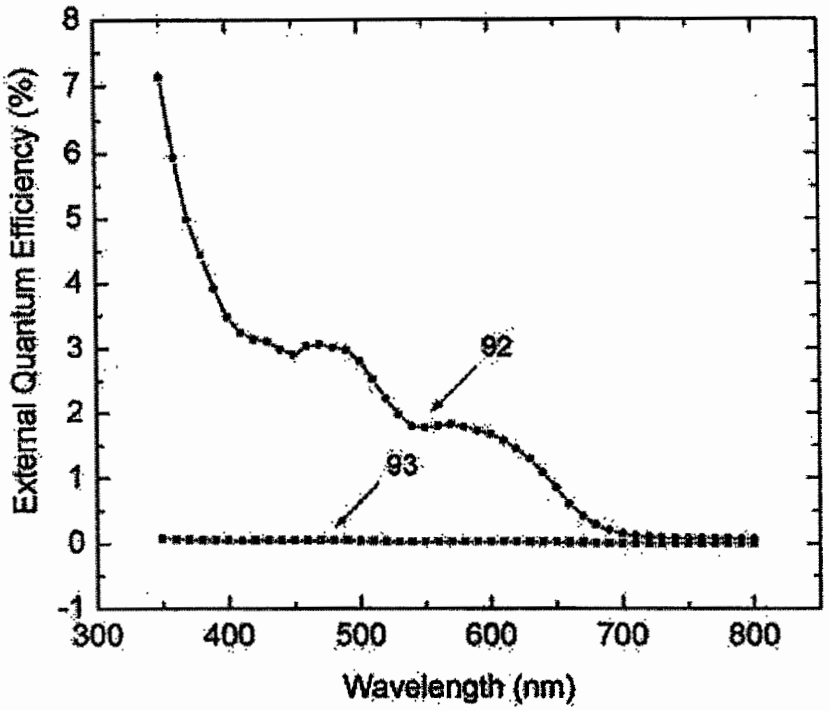

Figure 3.28 Comparison of Samples 92 and 93

Figure 3.28 compares Samples 92 and 93. The band diagram in Figure 3.9 shows that the band offsets for both Samples 92 and 93 are favorable for charge transfer. Thus the substantial improvement in efficiency between Samples 92 and 93 appears to be due to the incorporation of ZnO nanowires.

3.2 MEH-PPV Conductivity Over Time

Beyond attempts to optimize the annealing procedures and the layering scheme of the cell design, observations were made regarding the behavior of the samples with time. In particular, it was found that the absorption characteristics of MEH-PPV improve over time. The efficiency of Samples 81 and 84 were tested again, after 49 days and 27 days had elapsed, respectively, since the initial characterization. Both samples exhibited improved efficiency.

Initially, the measurements of the older samples were tested to determine if annealing the sample again would restore its original efficiency. We measured the efficiency of the best pads on each sample before and after re-anneal, as shown in Figures 3.29 and 3.30 (pg. 55). In each case (including additional results addressed in Tables 3 and 4 in the Appendix), the highest efficiency for each pad was obtained prior to the re-anneal, after a significant amount of time had passed since the original measurements. In addition, the efficiency decreases after the re-anneal, although the re-annealed efficiencies are still higher than the original efficiencies. In the case of Sample 81, the original magnitude of the MEH-PPV peak was 0.13%, whereas it increased to a magnitude of 0.23% after 49 days.

The improvement in the photoconductivity of MEH-PPV over time has been addressed in the literature. It is suggested that photo-oxidation defects and water vapor may create traps that cause the dissociation of excitons, thereby increasing the photocurrent as the oxygen/ water vapor content increases with time [34, 35]. This may explain why the photocurrent decreases when the device is heated in vacuum during the re-anneal. Exposure to oxygen, humidity and light, however, is also often cited as a source of degradation to MEH-PPV [5, 36-38]. In reviewing the literature, it is clear that oxygen content increases with time and that the effect of light, oxygen and water vapor have a significant impact on the optoelectronic properties of this polymer. It is also clear that the influence of these factors is a topic still under debate.

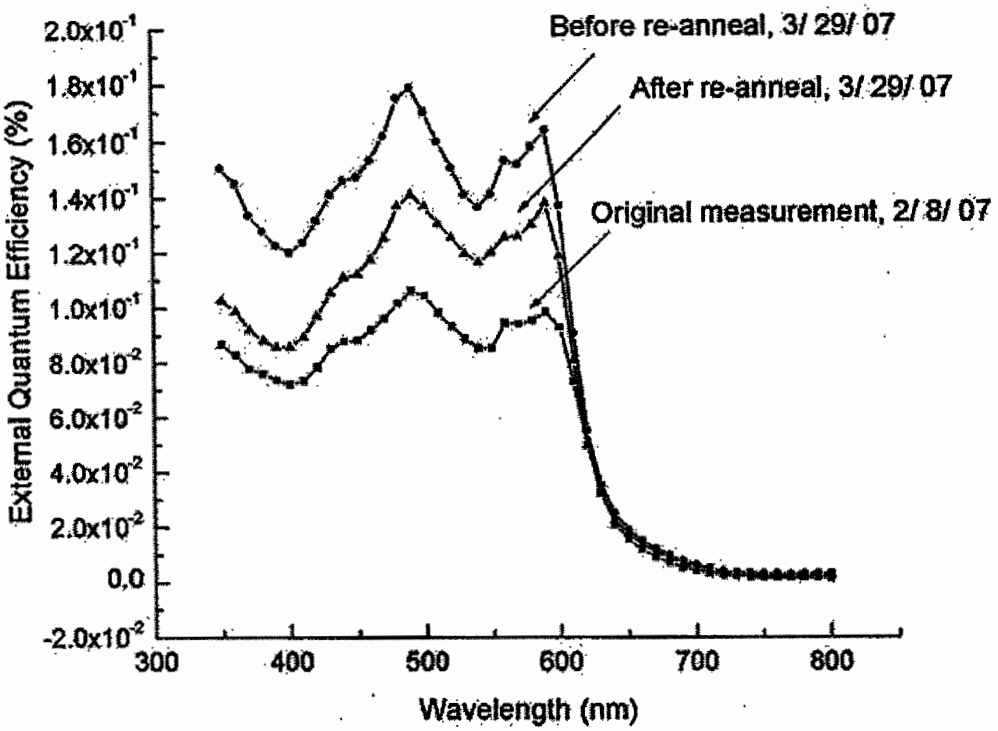

Figure 3.29 Sample 81 External quantum efficiency after 49 days and re-anneal

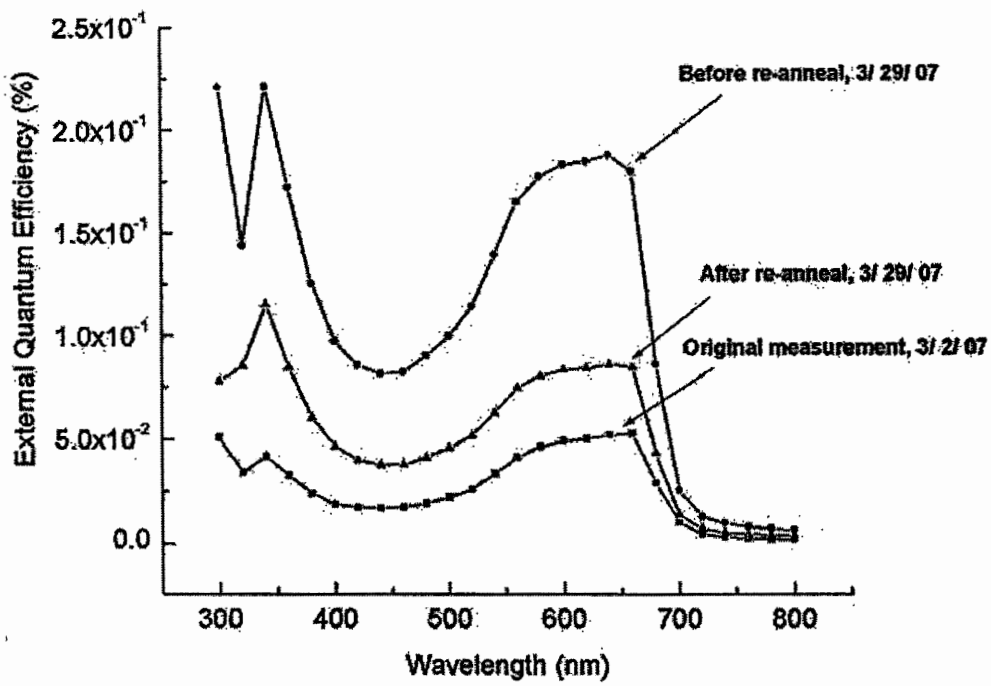

Figure 3.30 Sample 84 External quantum efficiency after 27 days and re-anneal

3.3 Future work

To improve rectification in the I-V curves, a different n-type material should be considered. The variety of n-type organic semiconductors available is limited, due to difficulties in fabrication procedures. It is possible, however, to further dope n-type organic materials with other n-type compounds [15, 17].

Alternatively, if the ZnO nanowires themselves could be heavily n-doped, this would avoid the necessity of the n-type organic semiconductor layer by forming the p-n junction directly between the nanowires and the p-type polymer. Heavily n-doping the ZnO nanowires would establish better band-bending at the interface between the nanowires and the p-type polymer, and thus improve charge transfer (See the energy band diagrams in Figures 3.2, 3.8 and 3.9). Other approaches could involve using metallic nanowires, or doping the inorganic quantum dots to obtain n-type properties.

In addition to optimizing band offsets, further improvements could be made by minimizing the polymer layer thickness. Thinner transport layers would allow a greater number of photogenerated carriers to reach the contacts, thereby increasing quantum efficiency.

4. Conclusions

We have fabricated a hybrid organic/ inorganic solar cell sensitized by the addition of CdSe quantum dots. Both MEH-PPV and CdSe absorb in independent ranges. Our results show that the quantum dot band gap can be tuned to optimize the absorption of the solar cell.

CdSe clearly maintains quantum dot characteristics. Although the ligands are removed at low temperature, the CdSe particles apparently do not agglomerate to form a bulk crystalline layer, despite the 430° C anneal. The isolation of the particles is evident in the observed absorption peaks, which are unique to the size and shape of the quantum dots. Since the particles are not in contact with each other, charge carriers photogenerated in the CdSe are transported through the matrix of the organic conductors.

The organic semiconductors were used to form a p-n junction. MEH-PPV, however, also behaved as an active absorption layer, and contributed substantially to the overall cell efficiency. The NTCDA, however, was reconsidered as the n-type wetting layer between CdSe and the ZnO nanowires. The most promising sample was fabricated without NTCDA, thereby indicating that this layer may have inhibited charge transfer in previous samples.

The ZnO nanowires were meant to provide a single-grain path from the absorber layers to the FTO. Our results indicate that the surface area enhancement provided by the ZnO nanowires improves charge transfer, when incorporated with materials that exhibit favorable band energy offsets. Open-circuit voltages of 0.45 V were obtained

and the maximum short circuit current was 1.5 x 10^{-6} A at 8 mW/ cm^2 white light intensity.

The cell design addressed herein could eventually be adapted to flexible substrates. ZnO nanowires could be grown by electrodeposition, and the solution-based processing of both the organic conductors and quantum dots could allow for large-scale ink-jet or screen printing methods, thereby offering a cost-effective alternative to the high temperature, high vacuum processing methods necessary for fabrication of the rigid silicon solar panels that are currently the industry standard.

REFERENCES

1. P. Würfel, Physics of Solar Cells, Wiley-VCH, 2005.

2. W. Shockley and H. Queisser, "Detailed Balance Limit of Efficiency of p-n Junction Solar Cells", *Journal of Applied Physics*, 1960.

3. M. A. Green, Third Generation Photovoltaics, Springer Verlag, 2003.

4. R. Könenkamp, et al., "Vertical nanowires light-emitting diode", *Applied Physics Letters*, 2004.

5. H. Neugebauer, et al, "Stability Studies and Degradation Analysis of Plastic Solar Cell Materials by FTIR", *Synthetic Metals*, 1999.

6. J. Halls, et al, "Efficient photodiodes from interpenetrating polymer networks", *Nature*, 1995.

7. G. Wallace, et al, "Conjugated polymers: New materials for photovoltaics", *Chemical Innovation*, 2000.

8. G. Schmid, Nanoparticles: From Theory to Application, Wiley-VCH, 2004.

9. P. Moriarty, "Nanostructured Materials", *Reports on Progress in Physics*, 2001.

10. S. Peulon and D. Lincot, "Mechanicstic Study of Cathodic Electrodeposition of Zinc Oxide and Zinc Hydroxychloride Films from Oxygenated Aqueous Zinc Chloride Solutions", *Journal of the Electrochemical Society*, 1998.

11. R. Könenkamp, et al., "Thin film semiconductor deposition on free-standing ZnO columns", *Applied Physics Letters,* 2000.

12. A. Nollau, et al, "Controlled n-type doping of a molecular organic semiconductor: Naphthalenetetracarboxylic dianhydride (NTCDA) doped with bis(ethylenedithio)-tetrathiafulvalene (BEDT-TTF)", *Journal of Applied Physics,* 2000.

13. G. Liang, et al, "Electrical characteristics of diodes fabricated with organic semiconductors", *Microelectronic Engineering*, 2002.

14. F. Li, *Novel dopants for n-type doping of electron transport materials: cationic dyes and their bases*, PhD thesis, Technischen Universität Dresden, 2005.

15. C.K. Chan, et al, "Molecular n-Type Doping of NTCDA by Pyronin B", Advanced Functional Materials, 2006.

16. J. G. Laquindanum, et al, "n-Channel Organic Transistor Materials Based on Naphthalene Frameworks", *Journal of the American Chemical Society,* 1996.

17. A. G. Werner, et al, "Pyronin B as a donor for n-type doping of organic thin films", Applied Physics Letters, 2003.

18. Breeze, A.J., et al, "Charge transport in TiO_2/ MEH-PPV polymer photovoltaics", *Physical Review B*, 2001.

19. Kang, H. S., et al, ".Electrical characterisitics of light-emitting diodes based on MEH-PPV derivatives: CzEH-PPV and OxdEH-PPV", *Synthetic Metals*, 2002.

20. Inigo, A. R., et al, "Disorder controlled hole transport in MEH-PPV", *Physical Review B*, 2004.

21. Kumar, A., et al, "Temperature and electric-field dependences of hole mobility in light-emitting diodes based on MEH-PPV", *Journal of Applied Physics*, 2005.

22. Bozano, L., et al, "Temperature- and Field-dependent electron and hole mobilities in light-emitting diodes", *Applied Physics Letters*, 1999.

23. Arango, A. C., et al, "Charge transfer in photovoltaics consisting of interpenetrating networks of conjugated polymer and TiO_2 nanoparticles", *Applied Physics Letters*, 1999.

24. Alam, M. M., et al, "Efficient Solar Cells from Layered Nanostructures of Donor and Acceptor Conjugated Polymers", *Chemistry of Materials*, 2004.

25. D. Shawf, et al, "The diffusion of chlorine in CdTe", *Solid State Physics,* 1984.

26. Takahashi, K., et al, "Performance Enhancement by Blending an Electron Acceptor in TiO_2/ polyphenylenevinylene/ Au Solid-state Solar Cells", *Chemistry Letters*, 2004.

27. Holt, A. L., et al, "Electrochemical and optical characterization of p- and n-doped MEH-PPV", *The Journal of Chemical Physics*, 2005.

28. T. Godinez, "Electroluminescence in nano-porous titania films", Master's Thesis, PSU, 2005.

29. B. Späth, et al, "Studies of sputtered ZnTe films as interlayer for the CdTe thin film solar cell", *Thin Solid Films*, 2005.

30. Y. Zhou, "Hybrid nanocrystal/polymer solar cells based on tetrapod-shaped $CdSe_xTe_{1-x}$ nanocrystals", *Nanotechnology,* 2006.

31. E. Kucur, "Determination of defect states in semiconductor nanocrystals by cyclic voltammetry", *Journal of Physical Chemistry, Series B*, 2005.

32. M. Jarosz, "The Physics and Chemistry of Transport in CdSe Quantum Dot Solids", PhD Thesis, MIT, 2004.

33. J. Chen, "Solution Properties of Single-Walled Carbon Nanotubes", *Science*, 1998.

34. M. Harrison, et al, "Analysis of the photocurrent action spectra of MEH-PPV polymer photodiodes", *Physical Review B*, 1997.

35. H. Antoniadis, et al, "Enhanced carrier photogeneration by defects in conjugated polymers and its mechanism", *Physical Review B*, 1994.

36. R. Khillan, et al, "The degradation of poly[2-methoxy-5-(2-ethylhexoxy)-1,4-phenylenevinylene] thin films studied by capacitance-voltage analysis and attenuated total reflection infrared spectroscopy", *Thin Film Solids,* 2005.

37. J. Scott, et al, "Degradation and failure of MEH-PPV light-emitting diodes", *Journal of Applied Physics,* 1996.

38. H. Radousky, et al, "Accelerated Degradation Studies of MEH-PPV", *27th International SAMPLE Technology Conference,* 1995.

39. http://www.nn-labs.com/

Appendix: Sample Results

Table 1: Summary of Prepared Solar Cells

Sample	Wavelength of Peaks (nm)	Magnitude (Photovoltage)	Rectification?
57 → 63: Optimizing MEH-PPV layer thickness			
Best Sample: 62 FTO/ ZnO/ MEH-PPV (6 layers, 10 g/ L)/ PEDOT-PSS (1 layer)/ Au	485	2.186×10^{-7}	No
64: ITO/ ZnO/ CdSe/ MEH-PPV (6 layers, 10g/ L)/ PEDOT-PSS (1 layer)/ Au	480	1.084×10^{-7}	No
65: ITO/ NTCDA (1 layer, 2 g/ L)/ MEH-PPV (1 layer, 2 g/ L)/ Al	NA	No Response	Pads shorted
66: ITO/ MEH-PPV (1 layer, 2 g/ L)/ NTCDA (1 layer, 2 g/ L)/ Al	NA	No Response	Pads shorted
67: ITO/ MEH-PPV (0.6% wt)/ NTCDA (0.6% wt)/ Al	460 340	1.2×10^{-7} 3.5×10^{-7}	Pads shorted
68: FTO/ ZnO/ CdSe/ MEH-PPV (6 layers, 10 g/ L)/ PEDOT-PSS (1 layer)/ Au	NA	No Response	Pads shorted
69: FTO/ ZnO/ CdTe (bulk, 52.3 g/ L)/ MEH-PPV (6 layers, 10 g/ L)/ Au	510 nm 835 nm	2.3×10^{-6} 5×10^{-7}	Yes, slight
70: FTO/ ZnO/ CdTe (bulk)/ NTCDA (1 layer, 10 g/ L)/ MEH-PPV (6 layers, 10 g/ L)/ Au	500 830	6×10^{-7} 2.5×10^{-7}	Yes, pronounced
71: FTO/ ZnO/ CdTe (bulk)/ NTCDA (1 layer, 10 g/ L)/ MEH-PPV (6 layers, 10 g/ L)/ Au	500 830	1.3×10^{-5} 5×10^{-7}	Yes
72: FTO/ CdTe (bulk)/ MEH-PPV (6 layers, 10 g/ L)/ Au	500 830	2.3×10^{-6} 7×10^{-7}	Yes, slight
73: FTO/ ZnO/ CdSe (d=3.4 nm)/ NTCDA (1 layer, 10 g/ L)/ MEH-PPV (6 layers, 10 g/ L)/ Au	500 620	10^{-6} 5×10^{-8}	Yes, slight

Sample	Wavelength of Peaks (nm)	Magnitude (Photovoltage)	Rectification?
74: FTO/ a-Si/ MEH-PPV (2 layers, 10 g/ L)/ Au	400 600	1.25×10^{-5} 6×10^{-6}	No
75: FTO/ ZnO/ a-Si/ MEH-PPV (2 layers, 10 g/ L)/ Au	600	1.1×10^{-7}	No
76: FTO/ ZnO/ a-Si/ Au	NA	No response	No
77: FTO/ a-Si/ au	400 560	1.1×10^{-5} 1.3×10^{-5}	No
78: FTO/ Al-doped ZnO/ CdSe (d= 3.4nm)/ NTCDA (1 layer, 10 g/ L)/ MEH-PPV (6 layers, 10 g/ L)/ Au	500 580	6.3×10^{-6} 7.4×10^{-6}	Yes, slight

Change in characteristics measured: Photovoltage → Photocurrent

Sample	Wavelength of Peaks (nm)	Magnitude (Photo-current)	Efficiency (%)	Rectification?
78: FTO/ Al-doped ZnO/ CdSe (d= 3.4nm)/ NTCDA (1 layer, 10 g/ L)/ MEH-PPV (6 layers, 10 g/ L)/ Au	500 580	5.8×10^{-11} 6.4×10^{-11}	2.2×10^{-2} 2.0×10^{-2}	Yes
79: FTO/ CdSe (d=3.4nm)/ NTCDA (1 layer, 10 g/ L)/ MEH-PPV (6 layers, 10 g/ L)/ Au	500 570	1.0×10^{-10} 1.1×10^{-10}	4.0×10^{-2} 3.6×10^{-2}	No
80: FTO/ Al-doped ZnO/ CdSe (d= 3.4nm)/ NTCDA (1 layer, 10 g/ L)/ MEH-PPV (6 layers, 10 g/ L)/ Au	500 600	1.3×10^{-10} 1.4×10^{-10}	5.0×10^{-2} 4.3×10^{-2}	Yes

Sample	Wavelength of Peaks (nm)	Magnitude (Photo-current)	Efficiency (%)	Rectification?
81: FTO/ Al-doped ZnO/ NTCDA (1 layer, 10 g/ L)/ CdSe (d= 5.8 nm)/ MEH-PPV (6 layers, 10 g/ L)/ Au	500 590	3.5×10^{-10} 4.0×10^{-10}	0.13 0.125	No
82: FTO/ Al-doped ZnO/ NTCDA (1 layer, 3 g/ L)/ CdSe (d= 5.8 nm)/ MEH-PPV (4 layers, 10 g/ L)/ Au ZnO Plasma Etched	590	2.3×10^{-10}	7.1×10^{-2}	No
83: Damaged	NA	NA	NA	NA
84: FTO/ Al-doped ZnO/ NTCDA (1 layer, 3 g/ L)/ CdSe (d= 5.8 nm)/ MEH-PPV (4 layers, 10 g/ L)/ Au NO Plasma Etch (Same design as 83)	640	1.7×10^{-10}	5.3×10^{-2}	Yes, slight
85: FTO/ Al-doped ZnO/ NTCDA (1 layer, 5 g/ L)/ CdTe (d= 5.2 nm)/ MEH-PPV (4 layers, 10 g/ L)/ Au	480	1.5×10^{-12}	6.5×10^{-4}	No
86: FTO/ Al-doped ZnO/ NTCDA (1 layer, 10 g/ L)/ CdSe (d= 5.8 nm)/ MEH-PPV (4 layers, 10 g/ L)/ Au No CdSe Anneal	490	3.5×10^{-11}	1.5×10^{-2}	No
87: FTO/ Al-doped ZnO/ PyB-doped NTCDA (1 layer, 5 g/ L NTCDA, 2 g/ L PyB)/ MEH-PPV (4 layers, 10 g/ L)/ Au	490	1×10^{-11}	5.5×10^{-3}	No
88: FTO/ Al-doped ZnO/ NTCDA (1 layer, 5 g/ L)/ MEH-PPV (4 layers, 10 g/ L)/ Au	490	9×10^{-11}	3.5×10^{-2}	No
89: FTO/ Al-doped ZnO/ NTCDA (10 g/ L)/ CdTe (d= 5.2 nm)/ MEH-PPV (4 layers, 10 g/ L)/ Au 300° C CdTe anneal	500	1.3×10^{-12}	1.3×10^{-3}	No
Sample	Wavelength of Peaks (nm)	Magnitude (Photo-current)	Efficiency (%)	Rectification?
92: FTO/ Al-doped ZnO/ CdSe (d=5.7 nm)/ MEH-PPV (6 layers, 10 g/ L)/ Au	490 580	7.4×10^{-9} 5.7×10^{-9}	3.1 1.82	No

Table 2: Sample 81 Time Elapse Test for MEH-PPV

81: FTO/ Al-doped ZnO/ NTCDA/ CdSe (d= 5.8 nm)/ MEH-PPV/ Au	Wavelength Peaks (nm)	Initial Efficiency (%)	Efficiency After 49 days (%)	Efficiency after re-anneal (%)
Pad 2	500 590	0.1 0.07	0.2 0.15	0.1 0.08
Pad 4	500 590	0.13 0.125	0.23 0.22	0.2 0.19
Pad 5	500 590	0.102 0.098	0.17 0.16	0.141 0.138

Table 3: Sample 84 Time Elapse Test for MEH-PPV

84: FTO/ Al-doped ZnO/ NTCDA/ CdSe (d= 5.8 nm)/ MEH-PPV/ Au	Wavelength Peak (nm)	Initial Efficiency	Efficiency After 49 days	Efficiency after re-anneal
Pad 2	640	0.05	0.19	0.09
Pad 4	640	0.05	0.07	0.06